

A Dynamical Study of a Cellular Automata Model of the Spread of HIV in a Lymph Node

E.G. Burkhead^a, J.M. Hawkins^{b,*}, D.K. Molinek^c

^a*Department of Mathematics and Computer Science, Meredith College, 3800 Hillsborough St., Raleigh, NC 27607, USA*

^b*Department of Mathematics, University of North Carolina at Chapel Hill, CB #3250, Chapel Hill, NC 27599-3250, USA*

^c*Department of Mathematics, Davidson College, P.O. Box 6999, Davidson, NC 28035, USA*

Received: 4 January 2008 / Accepted: 1 August 2008 / Published online: 30 August 2008
© Society for Mathematical Biology 2008

Abstract We conduct a mathematical study of a cellular automata model of the spread of the HIV virus in a lymph node. The model was proposed by Zorzenon dos Santos and Coutinho and captures the unique time scale of the viral spread. We give some rigorous mathematical results about the time scales and other dynamical aspects of the model as well as discuss parameter and model changes and their consequences.

Keywords Cellular automata · Dynamical systems · Virus spread

1. Introduction

In 2001, Zorzenon dos Santos and Coutinho published a description of a mathematical model of the spread of the human immunodeficiency virus (HIV) in a lymph node using cellular automata (Zorzenon dos Santos and Coutinho, 2001). We give a rigorous mathematical analysis of the model, and based on our results give some modifications. One of the most remarkable features of this model is its ability to reflect the clinical timing of the evolution of the virus in an individual; the typical progression of an HIV infection is illustrated in Fig. 1 (Fauci et al., 1996). Models are difficult to construct simulating the entire course of the infection due to several factors. While there is an overall pattern to the development of the infection, its progression varies among individuals infected with HIV. Additionally, several time scales are involved in the development of the disease: namely, there is a short term acute illness phase, measured in weeks, appearing soon after infection followed by a long term clinical latency period, lasting up to 10 years preceding a terminal illness. Most models are based on systems of ordinary differential equations and require different models for different stages of the infection (Nowak and May, 2000).

*Corresponding author.

E-mail addresses: burkhead@meredith.edu (E.G. Burkhead), jmh@math.unc.edu (J.M. Hawkins), domolinek@davidson.edu (D.K. Molinek).

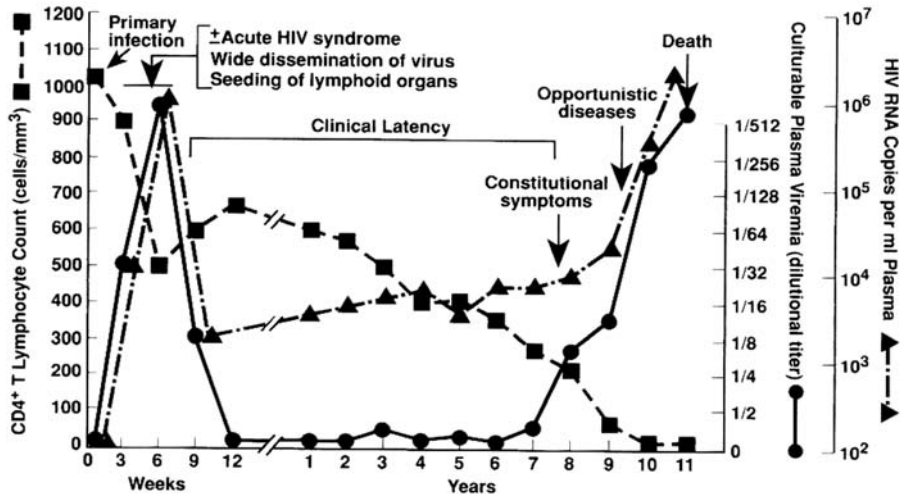


Fig. 1 Typical progression of HIV infection (reprinted with permission from *Ann. Int. Med.* (Fauci et al., 1996)).

Von Neumann and Ulam introduced cellular automata in the 1950s in an attempt to model a massively parallel and complex system such as the brain. While this early application was not successful, the mathematical framework endured and the subject developed much further in the hands of mathematicians, physicists, and other scientists. Cellular automata (CAs) give rise to many applications, and there is a copious literature on attempts to explain and classify the dynamics when a CA is iterated many times to simulate the passage of time. An overview of the literature can be found in several places, including Allouche et al. (2001), Kari (2005), or a general text on symbolic dynamics such as Kitchens (1998) or Lind and Marcus (1995). A large study of properties of cellular automata can be found in Wolfram's books (Wolfram, 1984, 2002), and for the various connections to physics a thorough source is Ilachinski (2001).

We use techniques from topological dynamics and ergodic theory to understand and generalize the model which was presented in Zorzenon dos Santos and Coutinho (2001) with minimal mathematical explanation. We prove statements about related models and parameter changes, but we do not attempt in this paper to make new biological predictions based on our findings. Where possible, we refer to primary sources in the literature for the medical and biological statements that we make. The new material lies in the mathematical approach to the study and the rigorous proofs supporting our analysis.

The paper is organized as follows. In Section 2, we give the definitions and preliminary results about cellular automata, focusing on stochastic CAs; we provide many examples to illustrate the concepts. We turn to the specific model at hand in Section 3, including some discussion connecting the mathematical choices made in the model with the underlying biology of the spread of HIV. We also give an explanation for the timing in the model supported by some numerical observations.

Sections 4 and 5 are concerned with proving mathematical results supporting statements made about the model in Section 3 and in the original paper (Zorzenon dos Santos and Coutinho, 2001). In the last section, Section 6, we discuss and demonstrate some

variations on the model reflecting current drug therapies. All programs used in this paper were written using Mathematica.

2. An overview of stochastic cellular automata

We begin with a finite state space (or alphabet) $\mathcal{A} = \{0, 1, \dots, m\}$ and for any integer dimension $d \geq 1$ we consider the lattice \mathbb{Z}^d , consisting of vectors $\vec{i} = (i_1, \dots, i_j, \dots, i_d)$, $i_j \in \mathbb{Z}$ for each $j = 1, \dots, d$. On \mathbb{Z}^d , we define $\|\vec{i}\| = \max\{|i_j|, j = 1, \dots, d\}$.

The space on which a cellular automaton is defined is the set of functions from \mathbb{Z}^d to \mathcal{A} , written

$$X = \mathcal{A}^{\mathbb{Z}^d},$$

and for each $x \in X$ and $\vec{i} \in \mathbb{Z}^d$, by $x_{\vec{i}}$ or $x_{(i_1, \dots, i_d)}$, we denote *the coordinate of x at \vec{i}* ; equivalently for each $\vec{i} \in \mathbb{Z}^d$, we obtain the canonical coordinate map $x \mapsto x_{\vec{i}} \in \mathcal{A}$. Because the notation is quite complicated in places, we will also use $[\cdot]_{\vec{i}}$ if there is a function of x inside the brackets whose coordinate at \vec{i} is needed. If $E \subset \mathbb{Z}^d$ is any finite set, by x_E , we denote the block of coordinates $\{x_{\vec{i}}, \vec{i} \in E\}$, i.e., $x_E \in \mathcal{A}^{|E|}$ where $|E|$ is the cardinality of E . We define a neighborhood of radius $k \in \mathbb{N} \cup \{0\}$ about $\vec{0} \in \mathbb{Z}^d$, by $N_k = \{\vec{i} = (i_1, \dots, i_j, \dots, i_d) : |i_j| \leq k\} = \{\vec{i} : \|\vec{i}\| \leq k\}$. Note that $|N_k| = (2k+1)^d$. Let u denote any fixed $(2k+1)^d$ pattern of symbols from \mathcal{A} , arranged in a $(2k+1) \times \dots \times (2k+1)$ d -cube centered at $\vec{0} \in \mathbb{Z}^d$. We define $B_u = \{x \in X : x_{N_k} = u\}$ to be a *cylinder of radius k* (centered at $\vec{0}$). B_u is precisely the set of points from X whose central block of coordinates extending out k units in each direction coincides with the fixed pattern u .

It is useful to describe a finite block of symbols u more generally and not necessarily centered at $\vec{0}$. A (*d -dimensional*) *pattern u* of size $k_1 \times k_2 \times \dots \times k_d$ is a set of symbols from \mathcal{A} arranged in a $(k_1 \times k_2 \times \dots \times k_d)$ -rectangular cube. By B_{u_0} , we denote the points in X which have the pattern u starting at $\vec{0}$ and extending in the positive direction in each dimension; i.e.,

$$B_{u_0} \equiv \{x \in X : x_{\vec{i}} = u_{\vec{i}}, 0 \leq i_j \leq k_M, M = 1, \dots, d\}.$$

Denoting $\vec{k} = (k_1, k_2, \dots, k_d)$, we define $E_{\vec{k}}$ to be the set in \mathbb{Z}^d such that

$$B_{u_0} = \{x : x_{\vec{i}} = u_{\vec{i}}, \vec{i} \in E_{\vec{k}}\}. \quad (1)$$

We define the shift action on X by: $\forall \vec{i} \in \mathbb{Z}^d$, $\sigma_{X, \vec{i}}(x)_{(j_1, \dots, j_d)} = x_{(j_1+i_1, \dots, j_d+i_d)}$, and denote it by σ_X . In order to discuss continuity of $\sigma_{X, \vec{i}}$, we need to define a metric on X . The metric we use on X is the classical one: $d_X(x, v) = \frac{1}{2^k}$ where $k = \min\{i : x_{N_i} \neq v_{N_i}\}$; X is compact with respect to the metric topology. This metric topology coincides with the Cartesian product topology.

Definition 2.1. A *d -dimensional cellular automaton (CA)* is a continuous map F on X such that for every $\vec{i} \in \mathbb{Z}^d$, $F \circ \sigma_{X, \vec{i}} = \sigma_{X, \vec{i}} \circ F$.

By work of Curtis, Hedlund, and Lyndon in the late 1960s (Hedlund, 1969), the following result allows us to characterize CAs by a local rule. The proof of this result follows from the definition of continuity in the metric topology on X .

Theorem 2.2 (Hedlund, 1969). *The map F on X is a CA if and only if there exists an integer $r \geq 0$ and a map $f : \mathcal{A}^{(2r+1)^d} \rightarrow \mathcal{A}$ such that for every $x \in X$,*

$$F(x)_i = f(x_{N_r+i}).$$

We call such a map f a *local rule* for the CA F . The integer r is called the *radius* of F . By using a larger alphabet if necessary and conjugating, we can assume that $r \leq 1$. However, we remain in the general case and use $r \geq 0$.

2.1. Stochastic CA

In the setting of interest, there are several CAs F_1, \dots, F_n acting on the same space X . At each iteration, we choose from among these CAs independently and randomly at each lattice site; the choices might not be equally weighted, but the probabilities are the same at each site.

We denote by J the finite index set (alphabet) with $|J| = n$, and let

$$\Omega = J^{\mathbb{N} \cup \{0\}}.$$

At each site in our integer lattice \mathbb{Z}^d , we choose randomly from among n different local rules for n cellular automata indexed by J . The random selection is modeled by the space (Ω, s) , the one-sided shift space with metric $d_\Omega(\omega, \zeta) = \frac{1}{2^k}$ where $k = \min\{i \mid \omega_i \neq \zeta_i\}$. We discuss probability measures on Ω in Section 2.2. For each $\omega \in \Omega$, we have the usual shift map

$$s(\omega)_j = \omega_{j+1}. \tag{2}$$

We now turn to the construction of a stochastic CA. Suppose we have n CAs F_1, \dots, F_n , on

$$X = \mathcal{A}^{\mathbb{Z}^d}$$

with associated local rules f_1, \dots, f_n , respectively, and assume each $F_j : X \rightarrow X$ has radius at most r .

We define the **stochastic cellular automaton** or **stochastic CA generated by F_1, F_2, \dots, F_n** on X as follows. On the space $\Omega \times \mathcal{A}^{(2r+1)^d}$, we define a local rule by: for each $x \in X$,

$$g(\omega, x_{N_r}) = \pi_{\mathcal{A}}(s(\omega), f_{\omega_0}(x_{N_r})) = f_{\omega_0}(x_{N_r}), \tag{3}$$

where $\pi_{\mathcal{A}}$ denotes projection onto the second coordinate (which is in \mathcal{A}). By definition

$$g : \Omega \times \mathcal{A}^{|N_r|} \rightarrow \mathcal{A}$$

and the rule g only depends on the 0th coordinate of ω .

We now look at an infinite product of the spaces Ω , by setting for each \vec{i} , $\Omega_{\vec{i}} = \Omega$, and defining

$$\overline{\Omega} = \prod_{\vec{i} \in \mathbb{Z}^d} \Omega_{\vec{i}}.$$

We denote each coordinate of a point by $\overline{\omega}_{\vec{i}} \equiv \omega^{(\vec{i})}$, noting that each $\omega^{(\vec{i})} = \{\omega_j^{(\vec{i})}\}_{j \in \mathbb{N} \cup \{0\}}$ is itself a one-sided sequence from Ω . On $\overline{\Omega}$, we have many possible shift maps, but we will focus on the one that performs the shift map of (2) coordinatewise; it is denoted \overline{s} and defined by:

$$[\overline{s}(\overline{\omega})]_j^{(\vec{i})} = \omega_{j+1}^{(\vec{i})} = [s(\omega^{(\vec{i})})]_j. \quad (4)$$

Finally, we define a random choice of local rule for each x and each infinite roll of the die $\overline{\omega} \in \overline{\Omega}$ by using Eq. (3):

$$[\overline{F}(\overline{\omega}, x)]_{\vec{i}} \equiv [F_{\overline{\omega}}(x)]_{\vec{i}} = g(\omega^{(\vec{i})}, x_{N_r + \vec{i}}) = f_{\omega_0^{(\vec{i})}}(x_{N_r + \vec{i}}). \quad (5)$$

For each \vec{i} , we consider only the coordinate $\omega^{(\vec{i})}$ of $\overline{\omega}$ and the coordinate block $x_{N_r + \vec{i}}$ to choose and apply one of the n local rules. We denote the stochastic CA by $F_{\overline{\omega}}$, and think of it as a process on X ; with this definition, $F_{\overline{\omega}}$ is not a true CA in the sense of Hedlund, but in Hawkins and Molinek (2007), it was shown to be closely related to one.

For each fixed pair $(\overline{\omega}, x)$, we iterate $F_{\overline{\omega}}(x)$ by:

$$F_{\overline{\omega}}^n(x) \equiv F_{\overline{s}^{n-1}\overline{\omega}} \circ \cdots \circ F_{\overline{s}\overline{\omega}} \circ F_{\overline{\omega}}(x). \quad (6)$$

We define a metric on the product space, $\Omega \times \mathcal{A}$ to be the maximum of the two coordinate metrics,

$$\delta((\omega, a), (\zeta, b)) = \max\{d_{\Omega}(\omega, \zeta), d_{\mathcal{A}}(a, b)\},$$

where $d_{\mathcal{A}}$ denotes the discrete metric on \mathcal{A} ; note that $\delta((\omega, a), (\zeta, b)) \leq 1$.

We then put the product structure on the space

$$Y = (\Omega \times \mathcal{A})^{\mathbb{Z}^d} = \overline{\Omega} \times X.$$

A point in Y has coordinates $y_{\vec{i}} = (\omega^{(\vec{i})}, x_{\vec{i}})$, for each $\vec{i} \in \mathbb{Z}^d$, with $\omega^{(\vec{i})} \in \Omega$, $x_{\vec{i}} \in \mathcal{A}$. The metric ρ on Y is given by:

$$\rho(y, z) = \sum_{k=0}^{\infty} \sum_{\|\vec{i}\|=k} \frac{\delta(y_{\vec{i}}, z_{\vec{i}})}{2^k}. \quad (7)$$

Since for each fixed k , the number of terms in the series is dependent upon the dimension in a polynomial way (e.g., if $d = 1$, we have 2 terms for each k , if $d = 2$, we have $8k$ terms, and for each dimension d , the number of terms added for each k is a polynomial of degree $d - 1$ in k), the series in Eq. (7) is finite and gives a metric. We remark that two points $y, z \in Y$ are close in the metric ρ if and only if the coordinates

$y_{\vec{t}} = (\omega^{(\vec{t})}, x_{\vec{t}})$ are close to the coordinates $z_{\vec{t}} = (\zeta^{(\vec{t})}, v_{\vec{t}})$ on some central block, say for all $\|\vec{t}\| \leq k$. This in turn means that $x_{\vec{t}} = v_{\vec{t}}$ for $\|\vec{t}\| \leq k$, and that $\omega_p^{(\vec{t})} = \zeta_p^{(\vec{t})}$ for $\|\vec{t}\| \leq k$ and for $p = 0, 1, \dots, t_{\vec{t}}$.

The shift map $\sigma_{Y, \vec{j}}$ on Y is defined for each $\vec{j} \in \mathbb{Z}^d$ by: $[\sigma_{Y, \vec{j}}(y)]_{\vec{t}} = y_{\vec{t} + \vec{j}} = (\omega^{(\vec{t} + \vec{j})}, x_{\vec{t} + \vec{j}}) \in \Omega \times \mathcal{A}$. The following proposition, stated and proved in Hawkins and Molinek (2007) in dimension 1, describes a continuous shift commuting map on a symbol space which represents the stochastic CA. The proof extends easily to arbitrary dimensions.

Proposition 2.3. *Assume we have n CAs F_1, \dots, F_n , on $X = \mathcal{A}^{\mathbb{Z}^d}$ with associated local rules f_1, \dots, f_n , respectively, such that each $F_j : X \rightarrow X$ has a radius bounded above by r . With the notation above, the map:*

$$\overline{F} : Y \rightarrow Y$$

defined using local rule:

$$\begin{aligned} \overline{g} : (\Omega \times \mathcal{A})^{|\mathcal{N}_r|} &\rightarrow \Omega \times \mathcal{A}, \\ \overline{g}(\omega^{(N_r)}, x_{N_r}) &= (s(\omega^{(\vec{0})}), f_{\omega^{(\vec{0})}}(x_{N_r})); \end{aligned} \quad (8)$$

so that

$$\overline{F}(y)_{\vec{t}} = \overline{g}(\omega^{(N_r + \vec{t})}, x_{N_r + \vec{t}}) = (s(\omega^{(\vec{t})}), f_{\omega^{(\vec{t})}}(x_{N_r + \vec{t}})) \quad (9)$$

is a continuous shift commuting map of Y .

Moreover, for each $x \in X$, and for each $\overline{\omega} \in \overline{\Omega}$,

$$[F_{\overline{\omega}}(x)]_{\vec{t}} = \pi_{\mathcal{A}_{\vec{t}}} \circ \overline{F}(y), \quad (10)$$

where $\pi_{\mathcal{A}_{\vec{t}}}$ denotes projection of $X = \mathcal{A}^{\mathbb{Z}^d}$ onto the copy of \mathcal{A} at the \vec{t}^{th} coordinate.

2.2. Measures on Ω and $\overline{\Omega}$

As above, our assumptions are that there are n CAs F_1, \dots, F_n with local rules f_1, \dots, f_n , respectively, each with a radius bounded above by r . We start with a probability vector $p = (p_1, \dots, p_n)$ where p_k indicates the probability that a random choice of one of the n CAs will yield F_k ; therefore, $p_k \geq 0$ and $\sum_{k=1}^n p_k = 1$. This in turn defines a measure on the σ -algebra of Borel sets in J , and hence an independently identically distributed measure μ on Ω characterized by: for each finite sequence, c_0, c_1, \dots, c_m , $\mu(\{\omega : \omega_k = c_k, k = 0, \dots, m\}) = p_{c_0} \cdot p_{c_1} \cdots p_{c_m}$. This is just the usual Bernoulli measure on Ω determined by the vector p and is invariant under the shift s . Using this measure on each $\Omega^{(\vec{t})}$, we obtain the canonical probability product measure $\overline{\mu}$ on $\overline{\Omega}$ preserved by \overline{s} .

The shift s is ergodic with respect to a probability measure μ if for any measurable function ϕ on Ω ,

$$\phi \circ s = \phi \text{ a.e.} \quad \Rightarrow \quad \phi = \text{constant a.e.}$$

It is well known that s is ergodic with respect to a Bernoulli measure μ , and we recall the following classical theorem (cf., e.g. Walters, 1982).

Theorem 2.4 (Birkhoff ergodic theorem). *If T on (X, μ) is a measure preserving the dynamical system, then for any $\phi \in L^1$, there exists $\phi^* \in L^1$ such that:*

1. $\lim_{n \rightarrow \infty} \frac{1}{n} \sum_{k=0}^{n-1} \phi \circ T^k(x) = \phi^*(x)$ μ -a.e.
2. $\phi^* \circ T(x) = \phi^*(x)$ μ -a.e.
3. $\phi^* \in L^1(X)$ and $\|\phi^*\|_1 \leq \|\phi\|_1$.
4. If T is ergodic and $\phi^* \in L^1(X)$, then $\phi^*(x) = \int_X \phi d\mu$.

If we consider a point $x \in X$ and look at one coordinate x_j ; at each time t , we roll an infinite die $\omega \equiv \omega^{(\vec{j})}$ to see which of the local CA rules to apply at that time and location. We define

$$A_i^T(\vec{j}, x, \omega) = \frac{\text{\#times } f_i \text{ is applied to } x_{N_t + \vec{j}} \text{ in first } T \text{ iterations}}{T}. \quad (11)$$

The following result tells us that assuming we run the stochastic CA long enough, we apply the CA F_i approximately 100 p_i % of the time for almost every ω .

Theorem 2.5. *For every $i \in \{1, \dots, n\}$, $\lim_{T \rightarrow \infty} A_i^T(\vec{j}, x, \omega) = p_i$ for any $x \in X = \mathcal{A}^{\mathbb{Z}^d}$, any $\vec{j} \in \mathbb{Z}^d$, and μ -a.e. $\omega \in \Omega_{\vec{j}}$.*

Proof: The result follows from Theorem 2.4 applied to s on Ω . In particular, let $C_i = \{\omega \in \Omega : \omega_0 = i\}$. By the Birkhoff ergodic theorem and the ergodicity of s with respect to μ ,

$$p_i = \mu(C_i) = \int_{\Omega} \chi_{C_i} d\mu = \lim_{T \rightarrow \infty} \frac{1}{T} \sum_{t=0}^{T-1} \chi_{C_i} \circ s^t(\omega) \quad (12)$$

for μ -a.e. $\omega \in \Omega$. By the definition of a stochastic CA, we have that

$$\begin{aligned} A_i^T(\vec{j}, x, \omega^{(\vec{j})}) &\equiv A_i^T(\vec{j}, \omega^{(\vec{j})}) = \frac{\#\{t : \omega_t^{(\vec{j})} = i\} \text{ for } 0 \leq t < T}{T} \\ &= \frac{\sum_{t=0}^{T-1} \chi_{C_i} \circ s^t(\omega^{(\vec{j})})}{T}, \end{aligned}$$

so by applying Eq. (12), we have that $\lim_{T \rightarrow \infty} A_i^T(\vec{j}, x, \omega) = p_i$ for μ -a.e. $\omega \in \Omega_{\vec{j}}$. The result is independent of x . \square

Corollary 2.6. *Given a stochastic CA as above, there exists a set $G \subset \overline{\Omega}$, $\overline{\mu}(G) = 1$ such that for every $\overline{\omega} \in G$, the following holds:*

$$\forall \vec{j} \in \mathbb{Z}^d, \forall x \in X, \quad \lim_{T \rightarrow \infty} A_i^T(\vec{j}, x, \omega^{(\vec{j})}) = p_i$$

with $\overline{\omega}_{\vec{j}} = \omega^{(\vec{j})}$.

Proof: The set of points ω for which Theorem 2.5 holds is independent of $\vec{j} \in \mathbb{Z}^d$ and of $x \in X$. \square

Other ergodic measures of interest for Ω are discussed in Sections 2.7 and 5. Unless otherwise specified, we assume that X is endowed with the σ -algebra of Borel sets and a Bernoulli product measure determined by the equal weighting of all states: $q = (1/|\mathcal{A}|, 1/|\mathcal{A}|, \dots)$.

2.3. Equicontinuity points of stochastic CAs

A point of equicontinuity in an iterated dynamical system is a point whose behavior can be predicted over time. This is one of the most important properties in this setting so we review the definition as given in Hawkins and Molinek (2007).

Recalling that $Y = (\Omega \times \mathcal{A})^{\mathbb{Z}^d}$ and that $\bar{F} : Y \rightarrow Y$ is defined by $\bar{F}(y)_{\vec{t}} = \bar{g}(\omega^{(\vec{t})}, x_{N_r+\vec{t}}) = (s(\omega^{(\vec{t})}), f_{\omega_0^{(\vec{t})}}(x_{N_r+\vec{t}}))$, we start with the definition of equicontinuity for this single transformation in order to give the definition for the associated stochastic CA $F_{\bar{\Omega}}$.

Definition 2.7 (Equicontinuity). Let $y, z \in (\Omega \times \mathcal{A})^{\mathbb{Z}^d}$ have coordinates $y_j = (\omega^{(\vec{j})}, x_j)$ and $z_j = (\zeta^{(\vec{j})}, v_j)$. Using the coordinates of y and z , we have the associated points $\bar{\omega}, \bar{\zeta} \in \bar{\Omega}$ and $x, v \in X$.

1. Recall that a **(single) CA** $F : X \rightarrow X$ is **equicontinuous at** $x \in X$ if $\forall \varepsilon = 2^{-k} > 0$, $\exists \delta > 0$ such that

$$d_X(x, v) < \delta \implies d_X(F^t(x), F^t(v)) < \varepsilon \quad \forall t \geq 0.$$

2. We say \bar{F} is **equicontinuous at** $y \in Y$ if $\forall \varepsilon = 2^{-k} > 0$, $\exists \delta > 0$ such that

$$\rho(y, z) < \delta \implies d_X(\{[F_{\bar{\omega}}^t(x)]_{\vec{t}}\}_{\vec{t} \in \mathbb{Z}^d}, \{[F_{\bar{\zeta}}^t(v)]_{\vec{t}}\}_{\vec{t} \in \mathbb{Z}^d}) < \varepsilon \quad \forall t \geq 0.$$

Note that the inequality for d_X holds if and only if

$$[F_{\bar{\omega}}^t(x)]_{\vec{t}} = [F_{\bar{\zeta}}^t(v)]_{\vec{t}}$$

for $\|\vec{t}\| \leq k$ and for all integers $t \geq 0$.

3. For any $\bar{\omega} \in \bar{\Omega}$ with $\bar{\omega}_{\vec{j}} = \omega^{(\vec{j})}$, we say the **stochastic CA** $F_{\bar{\Omega}}$ is **equicontinuous at** $x = \{x_j\}_{j \in \mathbb{Z}^d}$ if \bar{F} is equicontinuous at $y \in (\Omega \times \mathcal{A})^{\mathbb{Z}^d}$ with $y_j = (\omega^{(\vec{j})}, x_j)$.
4. We say that $F_{\bar{\Omega}}$ is **equicontinuous** if for every $\bar{\omega} \in \bar{\Omega}$, $F_{\bar{\omega}}$ is equicontinuous at x for every $x \in X$. This is equivalent to saying \bar{F} is equicontinuous at every $y \in Y$.
5. We define a CA $F : X \rightarrow X$ to be **almost equicontinuous** if the set of equicontinuity points contains a dense G_δ ; i.e., if the set of equicontinuity points can be written as the intersection of open, dense sets in X . We have the analogous definition for $\bar{F} : Y \rightarrow Y$ and we say the associated stochastic CA, $F_{\bar{\Omega}}$, is almost equicontinuous if \bar{F} is.

2.4. Blocking patterns and points of equicontinuity

For a single cellular automaton, the existence of a blocking pattern guarantees that the CA is almost equicontinuous; that is, the set of points of equicontinuity contains a dense G_δ . These patterns were introduced in Blanchard and Tisseur (2000) in dimension one and

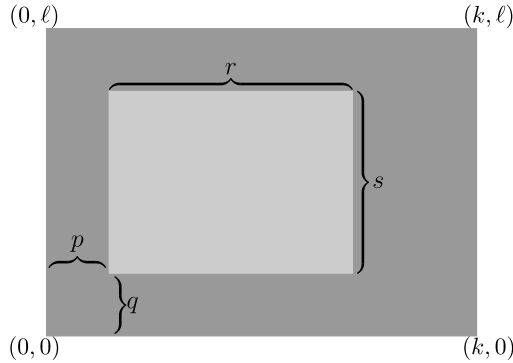


Fig. 2 A blocking pattern for a 2D cellular automaton.

generalized to higher dimensions by the first author in Gamber (2006). We first define blocking patterns in two dimensions; this is the setting in which we use it and the notation is simpler.

Definition 2.8. *Blocking patterns in $\mathcal{A}^{\mathbb{Z}^2}$:* A rectangular pattern u of size $k \times l$ is said to be (r, s) -**blocking** if there exist nonnegative integers $p \leq k - r$ and $q \leq l - s$ such that for all $x, y \in B_{u_0}$ and $t \geq 0$, we have

$$(F^t x)_{(i,j)} = (F^t y)_{(i,j)} \quad \forall i = p, \dots, p+r, \forall j = q, \dots, q+s. \quad (13)$$

The pair (p, q) is called the **offset**. That is to say, if the pattern u occurs in a point x at $\vec{t} + E_{\vec{k}}$, the coordinates of $F^t x$ on an $r \times s$ subset of $\vec{t} + E_{\vec{k}}$ are determined for all time t . See Fig. 2 for an illustration; the entire shaded region is an occurrence of u , and the lighter shaded region is the part which is determined for all time.

If $r = k$, $s = l$, and $p = q = 0$, we say that u is **fully blocking**. A fully blocking pattern is one whose occurrence in x at $\vec{t} + E_{\vec{k}}$ determines the coordinates of $F^t x$ at all vectors in $\vec{t} + E_{\vec{k}}$ for all time t .

Blocking patterns in $\mathcal{A}^{\mathbb{Z}^d}$ In higher dimensions, a pattern u of size $k_1 \times k_2 \times \dots \times k_d$ is (r_1, r_2, \dots, r_d) -**blocking** if the occurrence of u in a point x at $\vec{t} + E_{\vec{k}}$ determines the values of the coordinates of $F^t x$ in a $r_1 \times r_2 \times \dots \times r_d$ rectangular subcube in $\vec{t} + E_{\vec{k}}$ for all t . If each $k_i = r_i$, then u is said to be **fully blocking**; that is, the coordinates of $F^t x$ are determined at each occurrence of u in x , for all time t .

We mention some results relating blocking patterns to almost equicontinuous and equicontinuous CAs (see also Proposition 2.13).

Proposition 2.9 (Gamber, 2006). *Let $F : \mathcal{A}^{\mathbb{Z}^d} \rightarrow \mathcal{A}^{\mathbb{Z}^d}$ be a CA with radius r . If there exists a fully blocking pattern of size $k \times k \times \dots \times k$ for F , where $k \geq r$, then F is almost equicontinuous.*

Proposition 2.10 (Gamber Burkhead, 2008). *Let $F : X \rightarrow X$ be a cellular automaton with radius r , where $X \subseteq \mathcal{A}^{\mathbb{Z}^D}$. If there exists $L \geq r$ such that for all $\ell \times \cdots \times \ell$ patterns u where $\ell \geq L$, u is fully blocking, then F is equicontinuous.*

Propositions 2.9 and 2.10 each apply to a single CA. However, for a stochastic CA generated by F_1, \dots, F_n , if we have a pattern, u , which is fully blocking for each F_i and the sequence of patterns determined by u is the same under each F_i , then we obtain points of equicontinuity for the stochastic CA. Theorem 2.11 below extends earlier results of the authors (Hawkins and Molinek, 2007, Theorem 4.6).

Suppose we have a CA F with local rule f . We assume we have a fully blocking pattern $u \in \mathcal{A}^{E_{\vec{k}}}$ for F . By a slight abuse of notation we define, using Eq. (1):

$$f(u) \equiv [F(B_{u_0})]_{E_{\vec{k}}} \in \mathcal{A}^{E_{\vec{k}}}.$$

The notation f is used to underscore the fact that the application of the CA F to the blocking pattern u is purely local and does not depend on the location of u in a point x .

Theorem 2.11. *Let u be a fully blocking pattern for $F_j : \mathcal{A}^{\mathbb{Z}^d} \rightarrow \mathcal{A}^{\mathbb{Z}^d}$, $j = 1, \dots, n$ such that for each nonnegative integer t , $f_1^t(u) = f_2^t(u) = \cdots = f_n^t(u)$. Then for any $\bar{\omega} \in \overline{\Omega}$, the stochastic CA $F_{\bar{\omega}}$ generated by F_1, \dots, F_n has a point of equicontinuity, $\xi \in X$.*

Proof: Let $u \in \mathcal{A}^{k_1 \times \cdots \times k_d}$ be a fully blocking pattern for each CA F_j , $j = 1, \dots, n$, such that for each integer $t \geq 0$ the n sequences of patterns $\{f_j^t(u)\}_{t \geq 0}$, $0 \leq j \leq n$ are the same. By Definition 2.7, (1) and (2), given any $\bar{\omega} = \{\omega^{(\vec{i})}\}_{\vec{i}}$, we must construct a point of equicontinuity in Y for \bar{F} of the form $y_{\vec{i}} = (\omega^{(\vec{i})}, \xi_{\vec{i}})$. The idea of the proof is to construct a point in $\xi \in X$ which is a point of equicontinuity for each F_j and involves only the blocking pattern u ; the hypotheses imply this point works for each $\bar{\omega} \in \overline{\Omega}$. We now turn to the details of the proof.

Letting $\vec{e}_j = (0, \dots, 1, \dots, 0)$ denote the standard basis vector in \mathbb{Z}^d with a 1 in the j^{th} place, we consider the sublattice of \mathbb{Z}^d given by

$$\Lambda \equiv \left\{ \lambda = \sum_{j=1}^d a_j k_j \vec{e}_j, a_j \in \mathbb{Z} \right\},$$

and we tile \mathbb{Z}^d with cubes of size $k_1 \times \cdots \times k_d$, of the form E_λ , $\lambda \in \Lambda$, where $E_\lambda \equiv \lambda + E_{\vec{k}}$. In this way, we can write

$$\mathbb{Z}^d = \bigcup_{\lambda \in \Lambda} E_\lambda, \tag{14}$$

and the union is disjoint.

We construct a point $\xi \in X$ by repeating the pattern u at each E_λ . For each $\lambda \in \Lambda$, define $\xi_{E_\lambda} = u$; by Eq. (14), this uniquely determines ξ . Since u is fully blocking and by our construction, $[F_i^t(\xi)]_{E_\lambda} = f_i^t(u) = f_j^t(u) = [F_j^t(\xi)]_{E_\lambda}$ for all $1 \leq i, j \leq n$, for all $t \in \mathbb{N} \cup \{0\}$, and for all $\lambda \in \Lambda$.

For any $\bar{\omega} \in \overline{\Omega}$, the coordinates of $\bar{\omega}$ and ξ determine a unique point $y \in Y$, which we claim is a point of equicontinuity for \bar{F} . To prove the claim, given $\varepsilon > 0$, find $L \geq 0$ such

that $2^{-L} < \varepsilon$. We define finite sets $S \subset \Lambda$ and $E_S \equiv \bigcup_{\lambda \in S} E_\lambda$ such that $N_L \subset E_S$, and let $R = \max\{\|\vec{r}\|, \vec{r} \in E_S\}$; we then choose $\delta = 2^{-R}$.

Then if $z \in Y$ is such that $\rho(y, z) < \delta$, it follows that the coordinates $y_{\vec{r}} = (\omega^{\vec{r}}, \xi_{\vec{r}})$ are close to the coordinates $z_{\vec{r}} = (\zeta^{\vec{r}}, v_{\vec{r}})$, for $\|\vec{r}\| < R$; and in particular we have $\xi_{E_S} = v_{E_S}$. Therefore, by hypothesis, $[F_{\vec{\omega}}^t(\xi)]_{\vec{r}} = [F_{\vec{\zeta}}^t(v)]_{\vec{r}}$ for all $\vec{r} \in E_S$, and for all $t \geq 0$; i.e., for all $\|\vec{r}\| < L$. This proves the claim and the theorem. \square

2.5. Sensitive dependence on initial conditions for CA

Stochastic cellular automata with points of equicontinuity were shown to exist in Hawkins and Molinek (2007) by exhibiting a system satisfying the hypotheses of Theorem 2.11. However, it is much more likely that such a process has sensitive dependence on initial conditions so we review the definitions here.

In what follows $X = \mathcal{A}^{\mathbb{Z}^d}$ and each F, F_1, \dots, F_n is a CA on X with radii bounded above by r . All notation for \overline{F} and $F_{\overline{\Omega}}$ is as above.

Definition 2.12 (Sensitive dependence on initial conditions).

1. The CA $F : X \rightarrow X$ has **sensitive dependence on initial conditions** if $\exists \varepsilon = 2^{-k} > 0$ such that $\forall x \in X$ and $\forall \delta > 0$, there exist $v \in X$ and $t \geq 0$ such that

$$d_X(x, v) < \delta \quad \text{and} \quad d_X(F^t x, F^t v) \geq \varepsilon.$$

We sometimes say F has **SDIC** for short.

2. Analogously, we say the map \overline{F} has **sensitive dependence on initial conditions** if $\exists \varepsilon = 2^{-k} > 0$ such that $\forall y \in (\Omega \times \mathcal{A})^{\mathbb{Z}^d}$ and $\forall \delta > 0$, there exist $z \in (\Omega \times \mathcal{A})^{\mathbb{Z}^d}$ and integer $t \geq 0$ such that

$$\rho(y, z) < \delta \quad \text{and} \quad d_X(\{[F_{\vec{\omega}}^t(x)]_{\vec{r}}\}_{\vec{r} \in \mathbb{Z}^d}, \{[F_{\vec{\zeta}}^t(v)]_{\vec{r}}\}_{\vec{r} \in \mathbb{Z}^d}) \geq \varepsilon.$$

In this case, we say also that $F_{\overline{\Omega}}$ has SDIC.

Due to the positive expansivity of the shift on Ω most stochastic CAs exhibit sensitive dependence on initial conditions, including ones coming from CAs of radius 0.

We mention two results connecting sensitive dependence on initial conditions to equicontinuity.

Proposition 2.13 (Gamber, 2006). *Let $X \subseteq \mathcal{A}^{\mathbb{Z}^d}$ be a subshift and $F : X \rightarrow X$ be a cellular automaton with radius r which does not have sensitive dependence on initial conditions. Then there exists an (r, r, \dots, r) -blocking pattern for F .*

We note that this result does not necessarily imply the existence of points of equicontinuity except in dimension 1; a discussion of this can be found in Gamber (2006). The next result extends part of Kůrka (2001), Theorem 5.1 to our setting of stochastic CA.

Proposition 2.14 (Hawkins and Molinek, 2007). *If the stochastic CA $F_{\overline{\Omega}}$ has a point of equicontinuity then $F_{\overline{\Omega}}$ does not have sensitive dependence on initial conditions.*

2.6. Examples

We give some basic examples illustrating the properties of stochastic cellular automata defined in this section.

Example 2.15. This one-dimensional example was shown to be a stochastic CA with points of equicontinuity in Hawkins and Molinek (2007). It is comprised of two CAs acting on the space $X = \{0, 1\}^{\mathbb{Z}}$. The tables in the examples list the outcome in row 2 of the local rule applied to the symbol in the center of the triple in row 1 above it, if its nearest neighbors are the ones given.

(Sum-Product) Let $\mathfrak{P} : X \rightarrow X$ be a cellular automaton for X with radius 1 defined by the local rule

$$p(x_{(i-1,i,i+1)}) = (x_i + x_{i-1}x_{i+1}) \pmod 2.$$

The local rule table is:

000	001	010	011	100	101	110	111
0	0	1	1	0	1	1	0

This CA is equicontinuous (Kůrka, 2001).

(Majority) Let $\mathfrak{M} : X \rightarrow X$ be a CA for X defined by the local rule

$$m(x_{(i-1,i,i+1)}) = \left\lfloor \frac{(x_{i-1} + x_i + x_{i+1})}{2} \right\rfloor,$$

with $\lfloor \cdot \rfloor$ denoting the integer part:

000	001	010	100	011	101	110	111
0	0	0	0	1	1	1	1

The majority CA is almost equicontinuous (Kůrka, 2001).

We choose the probability vector $p = (1/2, 1/2)$ to determine a measure on $\overline{\Omega}$ to form $F_{\overline{\Omega}}$ (or equivalently \overline{F}) from \mathfrak{P} and \mathfrak{M} , so each of the two CAs is equally likely to occur. Each individual CA has a fixed fully blocking pattern 001100, so satisfies the hypotheses of Theorem 2.11. Obviously, any choice of vector p gives equicontinuity points. In Fig. 3, a zero is shown as a white square and a 1 is black; the top line represents a randomly chosen initial point $x = (\dots, x_{-1}, x_0, x_1, \dots)$, the line below it $F_{\overline{\Omega}}(x)$, the second line is $F_{\overline{\Omega}}^2(x)$, etc.

The presence of points of equicontinuity gives predictable and simple long term but nonconstant behavior in Fig. 3. This is classified as Class II behavior by Wolfram (1984).

Example 2.16. In this example, we illustrate the opposite extreme on the predictability scale, namely sensitive dependence on initial conditions—in fact, Bernoulli behavior. The space is $X = \{0, 1, 2\}^{\mathbb{Z}}$, and the three one-dimensional CAs are given by constant local rules (of radius 0): $f_0 \equiv 0$, $f_1 \equiv 1$, $f_2 \equiv 2$. In Fig. 4, we use the vector

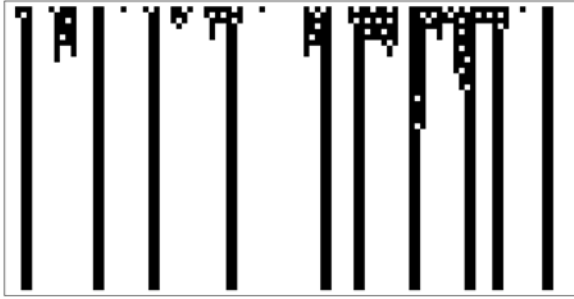


Fig. 3 A stochastic CA with equicontinuity points.



Fig. 4 Example 2.16 has sensitive dependence on initial conditions.

$p = (6/10, 3/10, 1/10)$ to generate μ and $\bar{\mu}$ on Ω and $\bar{\Omega}$, respectively, and the colors $0 = \text{white}$, $1 = \text{gray}$, and $2 = \text{black}$. Our initial x consists of all 1's, and it is clear from the definition that any point $\bar{\omega} \in \bar{\Omega}$ determines the dynamics completely; i.e., the process $F_{\bar{\omega}}$ is as random as the measure μ on Ω is, as this is repeated at each coordinate of $\bar{\Omega}$. Consequently, when we apply the stochastic CA once, we see the distribution of colors to be approximately 60% white, 30% gray, and 10% black. Using Definition 2.12, we show below that $F_{\bar{\omega}}$ has sensitive dependence on initial conditions with sensitivity constant $\varepsilon = 1$.

Lemma 2.17. *The stochastic CA given in Example 2.16 has sensitive dependence on initial conditions.*

Proof: By Definition 2.12, we show that \bar{F} has sensitive dependence on initial conditions with constant $\varepsilon = 1$. Given any $y \in Y$, $y_j = (\omega^{(j)}, x_j)$ and any $\delta = 2^{-L}$, we first choose $\bar{\zeta}$ so that $\zeta^{(j)} = \omega^{(j)}$ for all $j \neq 0$. We then set $\zeta_i^{(0)} = \omega_i^{(0)}$, $i = 0, 1, \dots, L$, and $\zeta_{L+1}^{(0)} \neq \omega_{L+1}^{(0)}$. Using z given by $z_j = (\zeta^{(j)}, x_j)$, these choices give rise to the points $y \neq z \in Y$ with $\rho(y, z) < \delta$. We see that

$$[F_{\bar{\omega}}^j(x)]_0 = [F_{\bar{\zeta}}^j(x)]_0, \quad j = 0, \dots, L + 1,$$

but that

$$[F_{\omega}^{L+2}(x)]_0 \neq [F_{\zeta}^{L+2}(x)]_0;$$

therefore, $d_X(\prod_{i=-\infty}^{\infty} (F_{\omega}^{L+2}(x))_i, \prod_{i=-\infty}^{\infty} (F_{\zeta}^{L+2}(v))_i) = 1$. \square

We generalize Example 2.16 to dimension d and show that it is isomorphic to a shift on a subset of $(d+1)$ -dimensional lattice space. In what follows, we denote $\mathbb{N}_0 \equiv \mathbb{N} \cup \{0\}$.

Example 2.18. Let $\mathcal{A} = \{0, 1, 2, \dots, n-1\}$ and $X = \mathcal{A}^{\mathbb{Z}^d}$, and define n d -dimensional CAs by the constant local rules: $f_j \equiv j$. Consider any probability vector $p = (p_0, \dots, p_{n-1})$, such that $p_j > 0$. We use the product measure determined by p , call it ν , on X . Also, on the die space $\Omega \equiv \mathcal{A}^{\mathbb{N}_0}$, we have the product measure μ which comes from p as well. We denote the resulting stochastic process by $F_{\overline{\Omega}}$; in this way we construct a stochastic CA on X with the corresponding map \overline{F} mapping $Y = (\Omega \times \mathcal{A})^{\mathbb{Z}^d}$ to itself given by, for every $i \in \mathbb{Z}^d$:

$$\overline{F}(y)_{\vec{i}} = (s(\omega^{(\vec{i})}), \omega_0^{(\vec{i})}). \quad (15)$$

The map \overline{F} has a particularly simple representation as a shift on the upper half space of $\mathcal{A}^{\mathbb{N}_0 \times \mathbb{Z}^d}$; this space is one dimension greater than that of X . This is described in the result below.

We can write any vector $\vec{v} \in \mathbb{N}_0 \times \mathbb{Z}^d$ as $\vec{v} = (j, \vec{i})$, with $j \in \mathbb{N}_0$ and $\vec{i} \in \mathbb{Z}^d$. Define \tilde{X} to be the set of all points $\tilde{y} \in \mathcal{A}^{\mathbb{N}_0 \times \mathbb{Z}^d}$ and write the coordinates as $\tilde{y}_{(j, \vec{i})}$, $j \in \mathbb{N}_0$, $\vec{i} \in \mathbb{Z}^d$. We think of \tilde{X} as one (of many) upper half spaces of $\mathcal{A}^{\mathbb{Z}^{d+1}}$.

Proposition 2.19. *The stochastic CA $F_{\overline{\Omega}}$ given in Example 2.18 is isomorphic to the shift $\sigma_{\vec{e}_1}$ on \tilde{X} using the independently identically distributed (i.i.d.) Bernoulli measure on \tilde{X} determined by p .*

Proof: We define a bijective map $\phi : Y \rightarrow \tilde{X}$ such that $\phi \circ \overline{F}(y) = \sigma_{\vec{e}_1} \circ \phi(y)$ for all y , and the measures on the two spaces are induced by the original probability vector p so it will be clear that ϕ is a measure preserving isomorphism. Consider any $y \in Y$, $\vec{i} \in \mathbb{Z}^d$, $y_{\vec{i}} = (\omega^{(\vec{i})}, x_{\vec{i}})$.

Writing $\tilde{x} = \phi(y)$, we define:

$$\tilde{x}_{(j, \vec{i})} = \begin{cases} x_{\vec{i}} & \text{if } j = 0, \\ \omega_{j-1}^{(\vec{i})} & \text{if } j \in \mathbb{N}. \end{cases} \quad (16)$$

We note that $[\sigma_{\vec{e}_1} \circ \phi(y)]_{(j, \vec{i})} = \tilde{x}_{(j+1, \vec{i})} = \omega_j^{(\vec{i})}$.

Suppose $\tilde{y} = \phi(\overline{F}(y)) = \phi(s(\omega^{(\vec{i})}), \omega_0^{(\vec{i})})$, then:

$$\tilde{y}_{(j, \vec{i})} = \begin{cases} \omega_0^{(\vec{i})} & \text{if } j = 0, \\ \omega_j^{(\vec{i})} & \text{if } j \in \mathbb{N}. \end{cases} \quad (17)$$

Since $\tilde{y}_{(j,\bar{\tau})} = \tilde{x}_{(j+1,\bar{\tau})}$, it follows that $\phi \circ \overline{F}(y) = \sigma_{\bar{e}_1} \circ \phi(y)$.

Clearly ϕ is injective, since if $y \neq z \in (\Omega \times \mathcal{A})^{\mathbb{Z}^d}$ with coordinates $y_{\bar{\tau}} = (\omega^{(\bar{\tau})}, x_{\bar{\tau}})$ and $z_{\bar{\tau}} = (\zeta^{(\bar{\tau})}, v_{\bar{\tau}})$; they must differ in some coordinate. This will be reflected in (16) so $\phi(y) \neq \phi(z)$. To show ϕ is surjective, we choose any $\tilde{x} \in \mathcal{A}^{\mathbb{N} \times \mathbb{Z}^d}$; since \tilde{x} is completely determined by its coordinates $x_{\bar{v}}$, we write: $\bar{v} \in \mathbb{N} \times \mathbb{Z}^d$ as $\bar{v} = (j, \bar{\tau})$, with $j \in \mathbb{N}$ and $\bar{\tau} \in \mathbb{Z}^d$. We then use Eq. (16) to define the individual coordinates $x_{\bar{\tau}}$ and $\omega_j^{(\bar{\tau})}$ and choose those points accordingly. Finally in each space, the measure of a cylinder is determined exclusively by its value on the fixed coordinates defining it, and this does not change under ϕ . \square

Corollary 2.20. *The map \overline{F} arising in Example 2.16 from $F_{\overline{\Omega}}$ is isomorphic to the shift $\sigma_{(1,0)}$ on the full shift half-space $\{0, 1, 2\}^{\mathbb{N}_0 \times \mathbb{Z}}$ using the i.i.d. Bernoulli measure on $\{0, 1, 2\}^{\mathbb{Z}^2}$. Moreover, $h(\sigma_{(1,0)}) = \infty$.*

Proof: We only need to prove the second statement. We use a result of Sinai (Sinai, 1994 p. 78, Lemma 3) for this; namely, since the entropy of the \mathbb{Z}^2 shift action, denoted σ_X earlier is positive then $h(\sigma_{(1,0)}) = \infty$. \square

Another useful generalization of our setting is the following: Suppose that we have defined a stochastic CA $F_{\overline{\omega}}(x)$ on X and $\Sigma \subset X$ is a closed shift invariant subset, i.e., for each $\bar{\tau} \in \mathbb{Z}^d$, we have $\sigma_{\bar{\tau}}\Sigma \subset \Sigma$. If in addition, we have that for each $\overline{\omega} \in \overline{\Omega}$ and for any $x \in \Sigma$, $F_{\overline{\omega}}(x) \in \Sigma$, then the stochastic CA is well defined on Σ . We call $(F_{\overline{\Omega}}, \Sigma)$ a **(stochastic) CA on a subshift**.

2.7. Markov measures

We define a Markov probability measure on Ω as follows. We consider a probability vector $p = (p_1, \dots, p_n)$ with $p_k > 0$ and a stochastic matrix $P = (p_{ij})_{i,j=1,\dots,n}$ (i.e., $p_{ij} \geq 0$ and all row sums are 1) such that $pP = p$. Then this defines a measure ν on Ω by: for each finite sequence c_0, c_1, \dots, c_m , $\nu(\{\omega : \omega_k = c_k, k = 0, \dots, m\}) = p_{c_0} \cdot p_{c_0 c_1} \cdots p_{c_{m-1} c_m}$. This measure ν is invariant for the shift s and we call (s, ν) the (p, P) -Markov shift.

We say the matrix P is *irreducible* if for each pair $i, j \exists l > 0$ such that $(P^l)_{ij} > 0$. The following classical result (cf. Walters, 1982) guarantees that Markov measures exist.

Theorem 2.21 (Perron–Frobenius theorem). *Let P be an irreducible stochastic matrix. Then 1 is an eigenvalue of P such that:*

1. 1 is a simple root of the characteristic polynomial of P .
2. 1 has strictly positive right and left eigenvectors.
3. These eigenvectors are unique up to constant multiple.
4. $1 \geq |\beta|$ for all other eigenvalues β of P .

The next several results play an important role in Section 5 since they provide a qualitative description of the long term dynamics of a Markov shift.

Lemma 2.22 (Walters, 1982, Lemma 1.18). *Let P be a stochastic matrix, having a strictly positive probability vector, p , with $pP = p$. Then $Q = \lim_{N \rightarrow \infty} \frac{1}{N} \sum_{n=0}^{N-1} P^n$ ex-*



Fig. 5 A stochastic CA using a Markov measure on Ω .

ists. The matrix Q is also stochastic and $QP = PQ = Q$. Any eigenvector of P for the eigenvalue 1 is also an eigenvector of Q and $Q^2 = Q$.

Theorem 2.23 (Walters, 1982, Theorem 1.19). *Let σ denote the (p, P) Markov shift. We can assume $p_i > 0$ for each i where $p = (p_0, \dots, p_n)$. Let Q be the matrix obtained in the previous lemma. The following are equivalent:*

1. σ is ergodic.
2. All rows of the matrix Q are identical.
3. Every entry in Q is strictly positive.
4. P is irreducible.
5. 1 is a simple eigenvalue of P .

Example 2.24. We generalize Example 2.18 further by putting a (p, P) Markov measure ν on Ω . On the state space $\mathcal{A} = \{1, 2, \dots, m\}$, $X = \mathcal{A}^{\mathbb{Z}^d}$ we have m CAs of radius 0 as above; each F_j is just the constant CA j so each local rule is simply $f_j \equiv j$. As before, $\Omega = \mathcal{A}^{\mathbb{N}_0}$. We fix a Markov measure ν as the measure for each factor in the infinite product space $\overline{\Omega}$. Let μ_p denote the i.i.d. Bernoulli product measure on X given by the vector p . In this way, we see that the process $F_{\overline{\Omega}}$ is isomorphic to running \mathbb{Z}^d simultaneous and independent trials of the same Markov process determined by the measure ν . This is discussed in more detail in Section 5 as it applies to our HIV model.

In Fig. 5, we show a one-dimensional Markov stochastic CA using three states (1, 2, 3) colored white, gray, and black, respectively, and a Markov measure determined by the pair (p, P) with $p = (2/5, 2/5, 1/5)$ and

$$P = \begin{bmatrix} \frac{1}{2} & \frac{1}{2} & 0 \\ 0 & \frac{1}{2} & \frac{1}{2} \\ 1 & 0 & 0 \end{bmatrix}.$$

We note that since the entries of $P = p_{ij}$ give the probabilities of going from state i to state j , once we see a 3 (black), for example, it can only be followed by a 1 (white) directly below it since $p_{32} = p_{33} = 0$.

We chose an initial point from X in Fig. 5 to be uniformly distributed among the 3 states (the top line shown in the grid). However, due to Theorem 2.23, the left eigenvector p for the eigenvalue 1 of P determines the measure μ_p on X toward which the CA asymptotically heads, and this shows in the bottom line in the grid of Fig. 5, where the statistical distribution of states looks more like $p = (2/5, 2/5, 1/5)$. This results in an invariant measure for the stochastic CA in the sense of the following result.

Proposition 2.25. *Suppose we have a finite alphabet $\mathcal{A} = \{1, 2, \dots, m\}$, the space $X = \mathcal{A}^{\mathbb{Z}^d}$, and m CAs given by $F_j = j$. Then with respect to any (p, P) Markov measure ν on Ω and the i.i.d. product measure $\overline{\mu}_p$ on X determined by μ_p on each coordinate of X , we have that \overline{F} is isomorphic to a the shift $\sigma_{(1, \overline{0})}$ on a subshift $\Sigma \subset \mathcal{A}_0^{\mathbb{N}} \times \mathcal{A}^{\mathbb{Z}^d}$ with respect to the invariant measure $\nu \times \overline{\mu}_p$ on Σ .*

Proof: The map ϕ given by Eq. (16) implements the isomorphism. The rest of the proof follows from a straightforward application of the definitions and pushing the Markov measures ν and $\overline{\mu}_p$, determined by (p, P) , forward to Σ . \square

3. The CA model of the dynamics of the viral spread

This section of the paper is organized as follows. We start with a mathematical description of the stochastic CA model used in Zorzenon dos Santos and Coutinho (2001), with minor modifications by the current authors, to model the spread of the HIV in a lymph node. We give some justification for choices of constants, with references. In Section 3.2, we give a more thorough biological justification and explanation for the physiological phenomena being simulated; we prefer to separate the biological statements from the mathematical analysis to the extent possible. We conclude this section with a preliminary analysis of how and why the model behaves as it does, combining the mathematical and biological statements in this discussion before turning to the rigorous mathematical results of Section 4.

3.1. The description of the model

We define our version of the mathematical model presented by Zorzenon dos Santos and Coutinho (2001). We use an alphabet $A = \{0, 1, \dots, m\}$ with $4 \leq m \leq 8$ depending on a parameter τ to be explained later. In particular, τ is chosen according to biological criteria and $m = 2 + \tau$; therefore, there are always $\tau + 3$ states. The space $X = A^{\mathbb{Z}^2}$ represents configurations of states of a lymph node (or other lymphatic tissue) as the lymphatic tissue contains most of the live HIV and is the location of the mutation of the virus as well as the $CD4^+ T$ (CD4 positive T helper) cells providing an immune response to the virus (Haase, 1999). Each coordinate of a point $x \in X$ represents one site on the lymph node comprised primarily of $CD4^+ T$ cells; the number and type of cells located at each coordinate could range from about 1 to 25 and could be macrophages or $CD4^+ T$ cells. We usually refer to this as a $CD4^+ T$ site instead of cell in order to avoid giving the impression, for example, that a single infected cell takes around 6 weeks to die after being infected (the usual figure given is ~ 2.6 days (Feinberg, 2002; Nowak and May, 2000)). In the original model, the term cell was used, but in Section 3.2, we show this cannot be literally the case with the

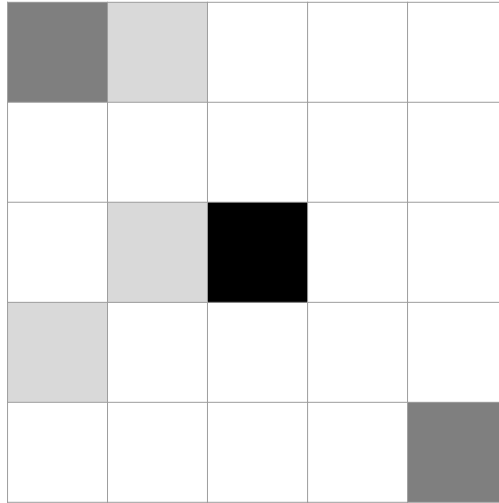


Fig. 6 One coordinate in our model is a small arrangement of cells representing up to 3 generations; this is one site (coordinate) in state 0 (healthy). Not every cell in the site is assumed to be in the identical state.

time step used (1 step = 1 week). We note that every cell in the same site might not actually be in the same state, but in any case, we apply one value 0 (healthy site) through m (dead or depleted cell site) to an aggregate of cells as shown, for example, in Fig. 6.

The decision to use dimension 2 instead of 3 is somewhat arbitrary; the entire setup for stochastic CA and some of our analysis on this model is done for any dimension. The justification for the original choice of dimension 2 is that the lymph node is more like a rough surface than a solid mass (Zorzenon dos Santos and Coutinho, 2001). Since there are estimated to be at least 10^{11} $CD4^+$ T cells in lymphatic tissue of an infected individual (Haase, 1999, p. 631), we carry out all of our analysis and prove theorems in Section 4 on an infinite grid, but computations made on finite square grids of side lengths 300 to 800 with periodic boundary conditions reflect the analysis reasonably well. In this paper, we show graphics run on a 700×700 grid (as a subset of \mathbb{Z}^2) using periodic boundary conditions in order to replicate the graphics in Zorzenon dos Santos and Coutinho (2001).

A time step in the model is a week, which is a compromise between the earliest dynamics of the disease measured in days and the long term course of the disease measured in years. With a choice of $\tau = 4$, there are 7 possible states for each coordinate of X . However, for every τ , the state 0 represents a healthy site, and the state m always represents a dead or depleted $CD4^+$ T site. The states 1 through $m - 1$ are split into two types: state $m - 1$ is always the final state of an infected site before it dies out (due to the immune system) and is called *infected-A2*; state 1 is always an infected site that has recently been infected, called a (newly) *infected-A1*. The other $\tau - 1$ states are recording the fact that a newly infected site takes τ time steps to go from infected-A1 to infected-A2; hence states 1 through $m - 2$ are sites each containing infected-A1 groups of cells along with some that were infected on the first day of the time step, died, were replenished, and re-infected. We assign different colors to the states 1 through $m - 2$, allowing us to see how long a site has been infected and when it is newly infected.

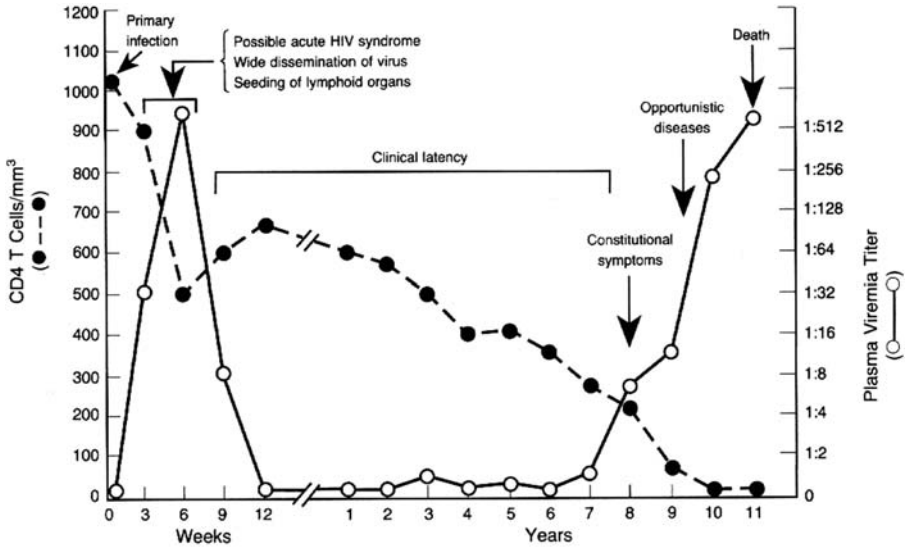


Fig. 7 Clinical data showing the progression of HIV infection (reprinted with permission from New England Journal of Medicine (Pantaleo, 1993)).

The lymph node is assumed to be all 0's before the experiment starts, and then the initial infection (at time $t = 0$) is represented as an initial percentage, written as p_{init} of newly infected-A1 $CD4^+$ T sites between 1 per 100 and 1 per 1,000 (Schnittman, 1989) coordinates of 1 with the rest being 0. We randomly infect $p_{\text{init}} \cdot 100\%$ of the sites throughout the grid (or a point $x \in X$). Our runs of the computer model use $p_{\text{init}} = .0055$ (the average), as well as $p_{\text{init}} = .01$ and $p_{\text{init}} = .001$. We compare our choices of p_{init} and graphical output with those of the original paper (Zorzenon dos Santos and Coutinho, 2001) below.

The observed time scales for the course of the HIV infection, given as ranges, are as follows (Nowak and May, 2000): After an initial infection, there is a sharp increase of the virus population during the first 2–8 weeks, usually peaking around week 8. This is followed by a sharp decline in the number of virus particles, hence the number of healthy $CD4^+$ T cells increases, and these levels last from 1 to 10 years; this is referred to as the clinical latency period, when a low level of virus is detected along with a gradual reduction in the number of uninfected $CD4^+$ T cells (during this clinical latency period a person infected with the virus typically has no symptoms). The third phase occurs when the percentage of $CD4^+$ T cells drops lower than around 30% (or less than 20% in the blood Nowak and May, 2000), and it is generally accepted that this leads to the onset of AIDS (acquired immune deficiency syndrome). In both the mathematical model and in the literature, while there is some disagreement over whether 20% or 30% defines AIDS, in both cases, the drop to the 30% level continues unabated to the 20% level or lower, and the final outcome is the same: an opportunistic infection takes hold due to the inability of the body to mount an immune response. In Fig. 7, we show the clinical picture of the timing based on data obtained by medical research discussed in Pantaleo (1993) and the references contained therein.

In the mathematical model, the final outcome is that there is a steady state of approximately $1/(m+1)$ healthy (state 0) coordinates in each point $F^t(x)$ as $t \rightarrow \infty$, but each coordinate is cycling through unhealthy and healthy states. Since this limiting behavior ranges from 11% to 20% of healthy cells as discussed in detail in Section 5, this is beyond what most clinical and lab data can show.

We present the local rules of the original model in Zorzenon dos Santos and Coutinho (2001) using the framework of a stochastic CA with 3 local rules. We now turn to the definition of the stochastic CA.

Using $\mathcal{A} = \{0, 1, \dots, m\}$, we define three local rules $f_1, f_2, f_3 : A^{3 \times 3} \rightarrow A$ as follows:

$$\begin{aligned}
 f_1, f_2, f_3 \left(\begin{array}{ccc} * & * & * \\ * & 0 & * \\ * & * & * \end{array} \right) &= \left\{ \begin{array}{l} 1 \text{ if } \geq 1 \text{ * is } 1, \dots, m-2, \text{ or if } \geq r \text{ *'s are } m-1\text{'s} \\ 0 \text{ otherwise,} \end{array} \right\}, \\
 f_1, f_2, f_3 \left(\begin{array}{ccc} * & * & * \\ * & a & * \\ * & * & * \end{array} \right) &= a+1 \quad \text{for } 1 \leq a \leq m-1, \\
 f_1 \left(\begin{array}{ccc} * & * & * \\ * & m & * \\ * & * & * \end{array} \right) &= 0, \quad f_2 \left(\begin{array}{ccc} * & * & * \\ * & m & * \\ * & * & * \end{array} \right) = 1, \quad f_3 \left(\begin{array}{ccc} * & * & * \\ * & m & * \\ * & * & * \end{array} \right) = m.
 \end{aligned}$$

Denote by $F_1, F_2, F_3 : \mathcal{A}^{\mathbb{Z}^2} \rightarrow \mathcal{A}^{\mathbb{Z}^2}$ the CA with local rule f_1, f_2, f_3 , respectively. The explanation of the CA rules is as follows:

1. For each $F_j, j = 1, 2, 3$, if a site in a healthy state (state 0) has an infected-A1 immediate neighbor, then it is updated to state 1 since it becomes infected-A1.
2. For each $F_j, j = 1, 2, 3$, if a site is infected-A1 or A2, so it is in state $a, a = 1, \dots, m-1$ at each time increment it is updated to state $a+1$. So, infected sites get eventually updated to A2 and then die (since state $m-1$ is updated to m). Recalling that we set $m = \tau + 2$, this is because τ represents the number of weeks it takes for an infected-A1 site to become an infected-A2 site (Zorzenon dos Santos and Coutinho, 2001): “Here τ represents the time required for the immune system to develop a specific response to kill an infected cell.” More discussion is below; basically, the primary sources show that a cell is killed within a few days, but a virus strain requires this amount of time to be destroyed by the immune response (see Section 3.2).
3. The parameter r represents the fact that an infected-A2 site is one which has already come under attack by the immune system and hence is less able to infect a neighboring site. A healthy cell should be touching at least r A2 sites before becoming infected. In this case, a 0 becomes a 1. The values for r range from 2 to 8; in Section 5, we give some supporting mathematical evidence that changing r has very little effect on the outcome in terms of the timing or the final equilibrium state of the model.
4. Once an infected site becomes depleted by the immune system responding to the infection, one of several things might occur. Most of the time the cells in the site are replenished and the state m is updated to a 0 (local rule f_1). However, some of the

time the cells are not replenished and the state of the site remains at m (local rule f_3), and other times the cells are replenished by a newly infected- $A1$ site (local rule f_2).

In our construction, $\Omega = \{1, 2, 3\}^N$ and it remains to give the probability vector $p = (p_1, p_2, p_3)$, which determines a measure $\bar{\mu}$ on $\bar{\Omega}$ for the resulting stochastic CA $F_{\bar{\omega}}$. Based on the discussion in the original paper (Zorzenon dos Santos and Coutinho, 2001), we use $p_1 = .9899901$, $p_2 = 9.9 \times 10^{-6}$, and $p_3 = .01$. The explanation for these choices is the following. Most of the time a depleted or dead $CD4^+T$ site is replaced by healthy $CD4^+T$ cells, hence p_1 should be very large. Approximately 1% of the time a site is not immediately replenished, hence $p_3 = .01$ since it represents the probability of a coordinate in state m being returned as an m again. A very small percentage of the cells replenished are with cells that are immediately infected, either because they have been circulating in the lymph system and occupy the space of a depleted site or because latently infected cells becomes active (Zorzenon dos Santos and Coutinho, 2001). Therefore, we choose p_2 to represent this tiny fraction of the time, and p_1 is just $1 - p_2 - p_3$. The connecting equations between the original notation (Zorzenon dos Santos and Coutinho, 2001) and ours are:

- 1) $p_{repl} =$ probability of replacing dead site with healthy.
 - 2) $p_{newinfec} =$ probability of replacing new healthy site with 1.
 - 3) $p_1 \equiv p_{repl} - p_{newinfec}$.
 - 4) $p_2 \equiv p_{newinfec}$.
 - 5) $p_3 \equiv 1 - p_{repl}$.
- (18)

Other choices made to run the model as in the original paper are: $r = 4$ and $\tau = 4$. In the next several figures, we show some graphical and numerical output of running the computer model. White squares are always healthy cell sites; the lightest blue (or gray) coordinates are the newly infected $A1$ cell sites, and then the sites get progressively darker as the state increases until finally at state 6, the darkest blue (black) states represent depleted sites.

In Figs. 8, 9, 10 and 11, we illustrate some typical behavior shown by the model, using a 700×700 grid. At the top of each large square, we list the number of weeks elapsed (20 – 566) followed by the percentage of healthy (white) sites remaining in the grid. Figure 8 shows a run using $p_{init} = .001$ which resulted in a clinical latency period of around 10 years; recall that each point in the grid represents one $CD4^+T$ cell site in a lymph node. Figure 9 graphically compares the percentage of healthy sites (solid black line), infected sites (dashed line), and dead sites (dotted line) vs. time in weeks for the run shown in Fig. 8. We note that the percentage of healthy cells has dropped below the threshold of 30% after 566 weeks (10.9 years, fairly long clinical latency period for both the model and an individual (Nowak and May, 2000)). In Figs. 10 and 11, we use $p_{init} = .0055$, $p_2 = 5.445 \times 10^{-5}$, resulting in much shorter clinical latency period, less than 5 years, which sometimes occurs in a clinical setting (Haase, 1999).

The parameters used in the original paper The values chosen above for the parameters in (18) are supported by the biological statements made in Zorzenon dos Santos and Coutinho (2001), Nowak and May (2000), and Schnittman (1989), but do not agree with the value $p_{init} = .05$ used in Zorzenon dos Santos and Coutinho (2001). While the intent of the authors may be to use $.001 \leq p_{init} \leq .01$, errors in Zorzenon dos Santos and

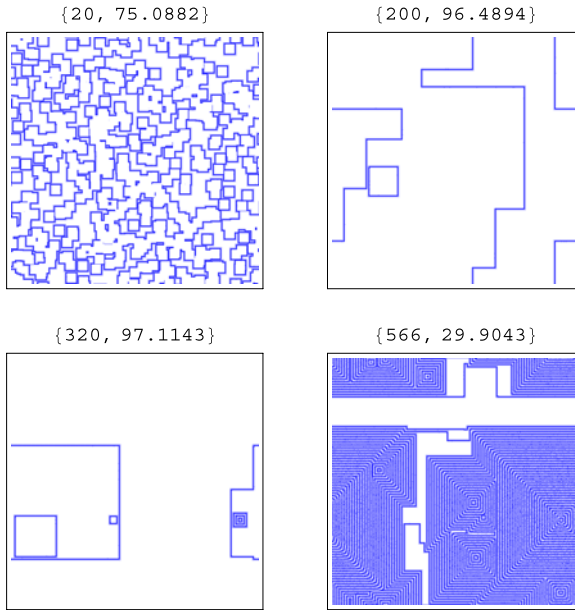


Fig. 8 The iteration of an initial point (e.g., configuration of a lymph node) under the CA.

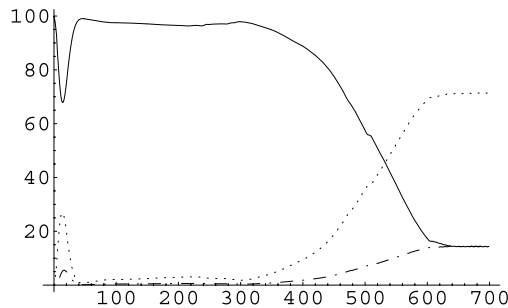


Fig. 9 The graphs showing percentage of healthy (black), infected (dotted), and dead (dashed) cell sites vs. weeks in Fig. 8.

Coutinho (2001) make it a bit difficult to determine the precise values used. The graphs showing the percentages of healthy, infected, and dead cell sites as a function of weeks after infection, starting from the value $p_{\text{init}} = .05$ and shown in Fig. 12, do not simulate the time scales discussed in the literature (cf. Nowak and May, 2000). More precisely, using the initial viral load of 5% ($p_{\text{init}} = .05$) gives output like that of Fig. 12 virtually all of the time instead of as outlying values; note also that the percentage of healthy sites drops to nearly 0 between 4 and 6 weeks after infection, which has no supporting clinical data. The data used for Fig. 12 comes from the grid simulation shown in Fig. 13. For each of the times $t = 5, 18, 25, 200$, we zoomed in on a small box in the upper left quadrant

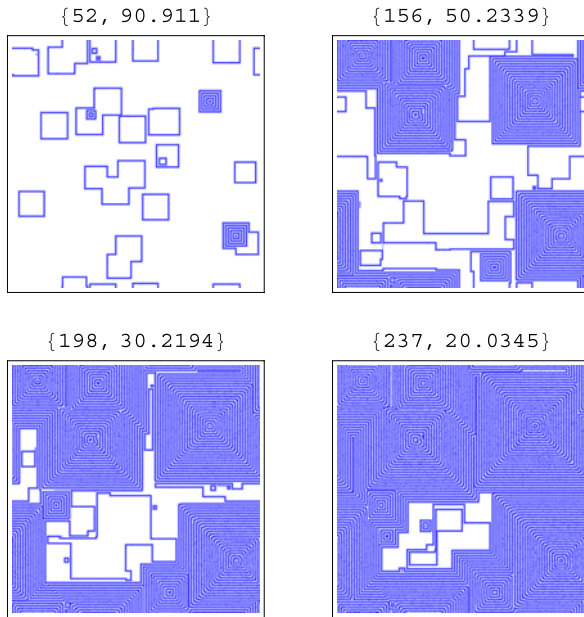


Fig. 10 The iteration of an initial point with a shorter clinical latency period.

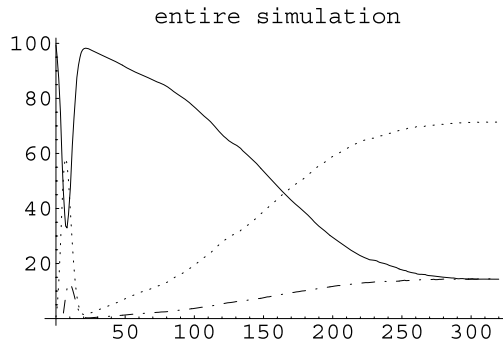


Fig. 11 The graph of the percentage of healthy, infected, and dead cell sites vs. time in weeks from Fig. 10.

to produce Fig. 14. We note that the graphical output shown in Zorzenon dos Santos and Coutinho (2001) and in Fig. 14 match closely.

We next compare this output with that of Fig. 15 which was run using $p_{init} = .0055$, or .55% of initially infected cells. While they appear to be very similar, looking at the source picture of Fig. 15, which is Fig. 16, we see a simulation agreeing more closely with clinical data and quite different from the output shown in Fig. 13. Finally, the primary reference given for the choice of p_{init} was incorrectly stated in Zorzenon dos Santos and Coutinho (2001), but using the (most likely intended) correct reference (Schnittman,

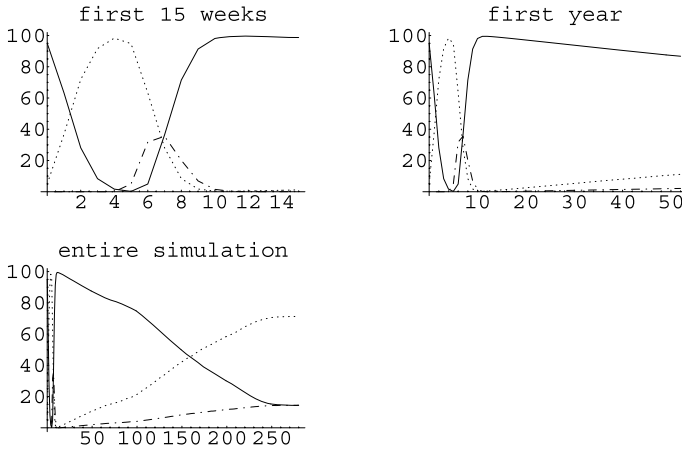


Fig. 12 The graph of the percentage of healthy (black), infected (dotted), and dead (dashed) cell sites vs. time in weeks, using $p_{\text{init}} = .05$.

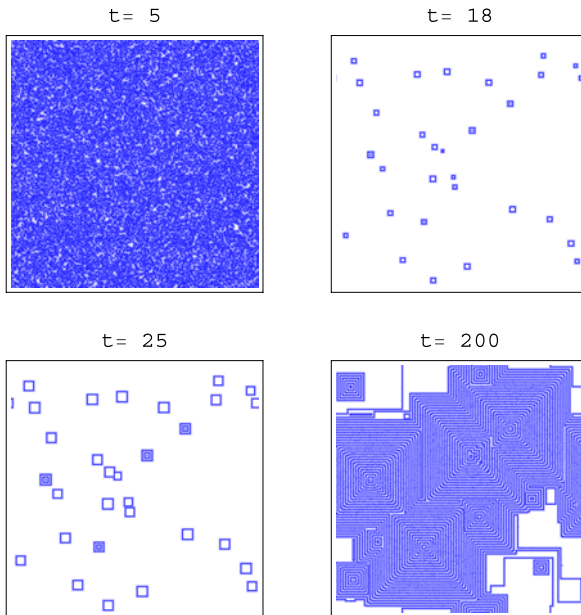


Fig. 13 Iterates of the model using $p_{\text{init}} = .05$ for initially infected cells.

1989), we see that indeed $.001 \leq p_{\text{init}} \leq .01$ seems to be the correct range from which to choose p_{init} .

To summarize, the local structure looks similar for different values of p_{init} ; this is shown by comparing last few boxes in Figs. 14 and 15, and in Section 4 is proved to be the case. However, the global and long term behavior revealed by comparing Figs. 12, 13,

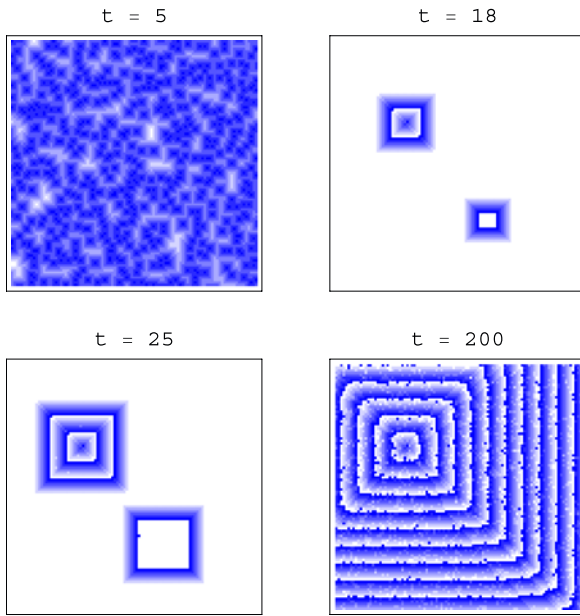


Fig. 14 Zooming in on each box in Fig. 13 replicates the grids in Zorzenon dos Santos and Coutinho (2001).

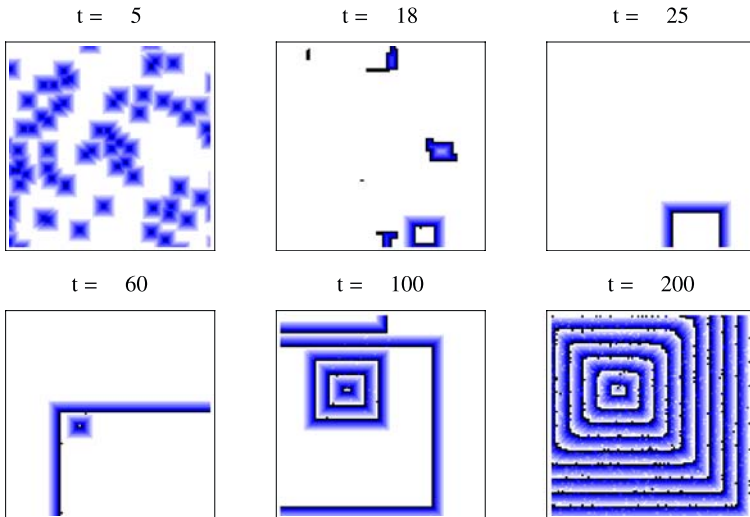


Fig. 15 We can also replicate the picture in Zorzenon dos Santos and Coutinho (2001) using an initial .55% of infected cells, or equivalently, $p_{init} = .0055$.

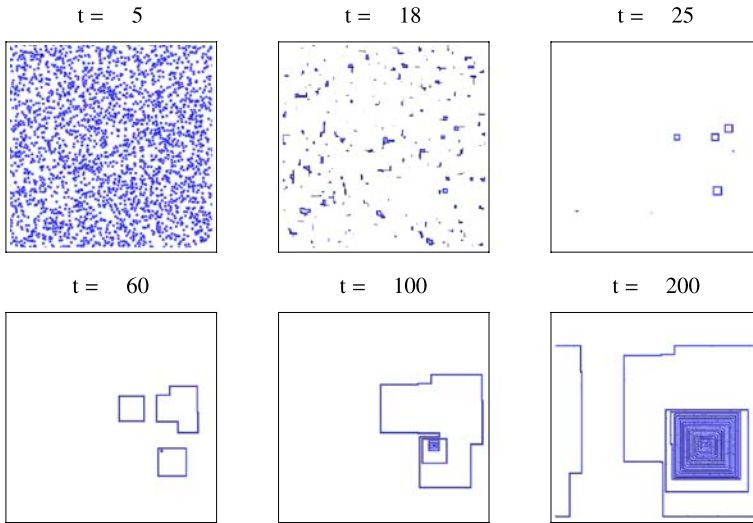


Fig. 16 Iterates of the model using $p_{init} = .0055$ for the initially infected cells.

and 16 show that the clinical latency period is drastically shortened by using the larger initial proportion of infected cells ($p_{init} = .05$).

Another variation we make on the original model based on the biological sources discussed in Section 3.2 below is that if a coordinate literally represents one $CD4^+ T$ cell, then one time step should be much shorter if indeed steps 1 through m take a cell from initial infection to death—more on the order of half a day than a week (Feinberg, 2002). Instead of shortening a time step, we use a coordinate to represent a small clump of cells, (for infected cells, it is usually 3 generations), exhibiting closely related behavior. Our terminology might be more accurately changed to “infectious”-A2 from “infected”-A2 cells since the site is indeed infectious while not every cell in it is necessarily infected (but we do not change the term). A cell that was infected by a strain of the virus at time $t = 0$ has been dead a very long time by $t = 6$; however, it remains in close proximity to cells recently infected by a genetically similar strain of virus not yet killed by the immune response, so as such forms part of an infectious-A2 site. The importance of A2 sites becomes apparent when we discuss the chronic and acute infection sources in Section 3.3 below.

3.2. Some biological notes about the model

The nature of HIV and its interaction with living cells are extremely complex. Models of the dynamics of HIV infection necessarily introduce major simplifications. We give some basic explanation here for choices made in the model of Zorzenon dos Santos and Coutinho (2001); in addition, we add explanation for our changes in the model. We make no attempt to convey the full picture of the spread of HIV so many details are left undiscussed, including some that may eventually be shown to affect the dynamics.

The cells of interest in this model, $CD4^+ T$ cells, represent one type of lymphocyte or white blood cell. There are varying estimates concerning the number of $CD4^+ T$ cells to

consider in this model, but the number given is usually between 10^{11} and 10^{12} ; in 1998, a reliable estimate was made in a controlled laboratory setting of 2.2×10^{11} (Zhang et al., 1998). Other estimates range from 10^{11} (Haase, 1999) $CD4^+$ T lymphocytes in lymphatic tissue in a person to 10^{12} (Nowak and May, 2000, p. 3) including CD^+4 , CD^+8 , and B-cells. The $CD4^+$ T cells in the lymph comprise 98% of the lymphocytes in the human body; the remaining 2% circulate in the blood (Zhang et al., 1998; Nowak and May, 2000, p. 3). The $CD4^+$ T cells control the immune system and are the cells infected by the introduction of HIV into the system; more precisely, the virus attaches itself to a receptor on a host $CD4^+$ T cell, inserts its RNA into the host cell, and manipulates the host cell into producing and releasing thousands of virus particles from its surface, usually killing the host cell in the process (Nowak and May, 2000, p. 12).

This leads to two notable features in the CA model, and also in this paper. The first is that we use the space X to represent some lymphatic tissue with each coordinate one $CD4^+$ T site; one can think of a lymph node, for example, and the number of cells is treated as infinite for the purposes of much of our mathematical analysis. The second is to ignore, in some sense, the number of viral particles; there is some mathematical and biological justification for this, namely that the number of free virus can be thought of as proportional to the number of infected cells (Nowak and May, 2000, p. 101). The validity of this assumption stems from the fact that most of the newly created virus particles decay and the number that remain are highly dependent on the number of available $CD4^+$ T host cells. A good mathematical model should reflect the clinical findings that the higher the initial viral load, the faster the disease progresses (Schnittman, 1989), which is equivalent to saying the faster the number of infected $CD4^+$ T cells increases. This model shows this over the course of many runs and the fact that each individual run of the model is somewhat unpredictable in terms of the growth of the infected cell population also agrees with the unpredictability of the disease progression in any one individual.

At some point soon after the introduction of HIV into the system of an individual, $CD4^+$ T cells start to become infected. The precise timing on this is controversial, but there is a consensus that after an initial viral explosion, the first detectable virus load in an infected person is anywhere from 1 per 100 to 1 per 1,000 (Schnittman, 1989); more precisely, this is the proportion of infected cells in the lymph nodes (Schnittman, 1989), which as mentioned above is much smaller than the actual viral dose. This model does not take into account what seems to be an initial exponential growth in the virus that occurs rapidly and then settles down to this measurable amount, which might take 5 to 10 days in all (Nowak and May, 2000). Since we are using infected $CD4^+$ T cells and not viral count, *we assume the initial conditions take place after the virus has stopped its initial fast growth and we begin the model ($t = 0$) at the "set point" of the viral infection.* This means that we assume the number of initial coordinates that are 1's is between .1% and 1%, randomly distributed among whatever grid size we use. However, a note expressing reservations about this model has pointed out this as a discrepancy (Strain and Levine, 2002), though we feel that this is mathematically a natural set of initial conditions. There are other subtle considerations about the earliest stages of the infection (Feinberg, 2002); in particular, it is known that macrophages in addition to $CD4^+$ T cells are infected early on, but scientists agree that infected $CD4^+$ T cells are by far the most prevalent HIV-infected cells in the lymphatic system (Haase, 1999).

Once newly created virus escapes from a host cell, the particles mature and attach to neighboring cells (Nowak and May, 2000). The number of nearby cells is unknown, and

it is somewhat arbitrary to choose 8—each neighbor in a two-dimensional neighborhood. Ranges from 3 to 11 and between 7 and 34 are mentioned in the literature (Nowak and May, 2000), but the larger number seems to incorporate extra time steps in our model so the value used seems to be a reasonable value.

Opportunistic infection which characterizes AIDS usually takes place when the $CD4^+ T$ counts fall to 200 per μl , which is around 20%. Generally an individual becomes symptomatic from an infection when the $CD4^+ T$ count is at 30%; a patient is currently diagnosed with AIDS when the $CD4^+ T$ count is less than 200 even if no symptoms are present (Nowak and May, 2000, p. 12). Even though the model is of dynamical activity in the lymph nodes, often counts in the blood are used to indicate this activity. Samples of lymphatic tissue are not easily or routinely obtained in an already immunologically compromised individual; however, the correlation seems to be widely accepted (Pantaleo and Fauci, 1996).

The short-term dynamics on the level of days or hours is somewhat obscured or at least hugely simplified by the stochastic CA model used. The half-life of virions (active circulating virus) is at most 6 hours. The time delay between the infection of a cell and its death or depletion is on the average 2.6 days, with a half-life of about 1.6 days (Feinberg, 2002); cells that have been infected longer have a higher chance of dying and that it is akin to an aging process of the cells. A generation of infection, the time from the release of a virion from an infected cell until it infects another cell causing it to release a new batch of virus is around 2.5 days, with an infected cell producing virus for only about 2 days. Therefore, in one time step of our current model, 7 days, there are around 3 generations of cell infections, three times more than the one shown. So why the choice of time step? At a given location in the lymph tissue, the immune response takes around τ weeks to be mounted against the local virus. And since we are looking at the global long term population dynamics of $CD4^+ T$ cells in the lymph tissue, a time step of a week is a natural compromise between the daily battles being waged between virus and immune system and the global health of the system which deteriorates on the order of years.

HIV makes many transcription errors and as a consequence mutates with great frequency (Nowak and May, 2000, Chap. 12); additionally, studies show that the invasion of a healthy $CD4^+ T$ cell by a virus particle is not the only cause of the depletion or death of cells (Feinberg, 2002). It takes some time for an immune response to be mounted against a virus and some cells die in a delayed manner for unknown reasons. Therefore, an infected cell remains able to infect its neighboring cells for several days, while the immediate region around the cell contains more infected cells and remains infectious for weeks. We accept for this model that τ is a reasonable estimate for an immune response to kill one particular strain of virus; i.e., the mutation rate causes the immune response to be a local response since each infected cell can be considered to be carrying a genetically distinct virus, sometimes referred to as a viral quasispecies (Nowak and May, 2000, Chap. 8: What is a quasispecies?).

The value of p_2 , the probability of replenishing a depleted site with an infected cell (which then infects the site within a week), while small, reflects the clinically supported hypothesis that there are reservoirs of latently infected $CD4^+ T$ cells that can spring into action at seemingly random times (Feinberg, 2002) along with the fact that with about 2% of these cells circulating, an infected cell might take the spot of a recently depleted one instead of being replaced by a healthy one (Pantaleo and Fauci, 1996).

The finer structure of the $CD4^+ T$ cell life and death cycle can be worked into the model using a procedure commonly used in symbolic dynamics called state splitting (see e.g. Lind and Marcus, 1995). In this scenario, a single cell in the current model would be recoded as 3 generations of cells, or say 9 states, and each time step would be reduced to 2.33 days instead of 7 days (one-third of a week). It is not apparent at this time that extra information would be gained from using a 63-state model (or more precisely $9 \cdot (\tau + 3)$ instead of the current $\tau + 3$ states), so we preserve the simplicity of the model with only a minor sacrifice in accuracy of the representation of the process modeled. There are other math models which focus more on the viral life and death cycles than on the $CD4^+ T$ cycles, and they use time increments of 8 hours (Bernaschi and Castiglione, 2002).

3.3. Preliminary explanation for how the models works

3.3.1. Phase 1. The early acute illness stage

Due to the probability vector used to determine the choice of local rule, $p = (p_1, p_2, p_3)$, it is clear that during the early stages the CA F_1 is exerting its influence essentially 99% of the time. Since F_1 basically models the evolution of a virus in a healthy person (albeit on a different time scale), and as we see from Proposition 4.3 in the next section, initial points of all 0's and 1's all tend to the completely healthy condition (the point $x = \bar{0}$ as $t \rightarrow \infty$). Therefore, this is qualitatively the dynamics observed at first.

We examine closely how the stochastic CA works on an initial point consisting of only 0's and 1's. We will work with $\tau = 4$; for the first 5 weeks, or when $t \leq \tau + 1$ weeks, each of the component CAs acts the same way since there are no 6's appearing. Therefore, the behavior is completely deterministic and the number of unhealthy sites grows quadratically in t ; if there are k_0 infected sites in a grid at time 0, assuming they are rather sparsely distributed; that is, under the assumption of no collisions, there are $k_0(2t + 1)^2$ infected or dead sites after t iterations of the model. This acts as a good upper bound for the computer runs. In Fig. 17, we show a comparison at the early time steps between the actual number of infected sites in a grid (shown as a solid line) superimposed on the (dashed) graph of the function $k_0(2t + 1)^2$ where k_0 is chosen to be the actual number of initially infected sites (which varies as p_{init} varies). The horizontal axis represents t in weeks. At $t = \tau + 1$ a (local) maximum number of unhealthy sites is approached, the original k_0 infected sites are depleted, and the next iteration of the model will replenish each with a healthy site with probability $p_1 \approx .99$. (We ignore the $\sim 1\%$ behavior for the moment though it plays a large role later and is a very real consideration in the progression of the disease (Zorzenon dos Santos and Coutinho, 2001).)

The timing on the maximum number of nonhealthy sites could vary by several time units depending on the distance of the initial infected sites to each other. If they are quite sparsely scattered, then when their centers are becoming healthy again ($t = \tau + 2$), outer rings of infected-A1 sites are being formed, creating more unhealthy sites than are being destroyed. If the initial state 1 coordinates are closer together than $2(\tau + 2)$, then intersections of squares of infected sites put a limit on the increase of infected sites. The restored centers of squares are surrounded by sites in state 6 (or $m = \tau + 2$); these sites cannot infect healthy sites so these interior squares in state 0 grow until virtually all the coordinates are healthy.

If there were no "1%" behavior, the system would return to a completely healthy state (this is Theorem 4.3 in the next section). But instead, the rare occurrence of F_2 and F_3 is

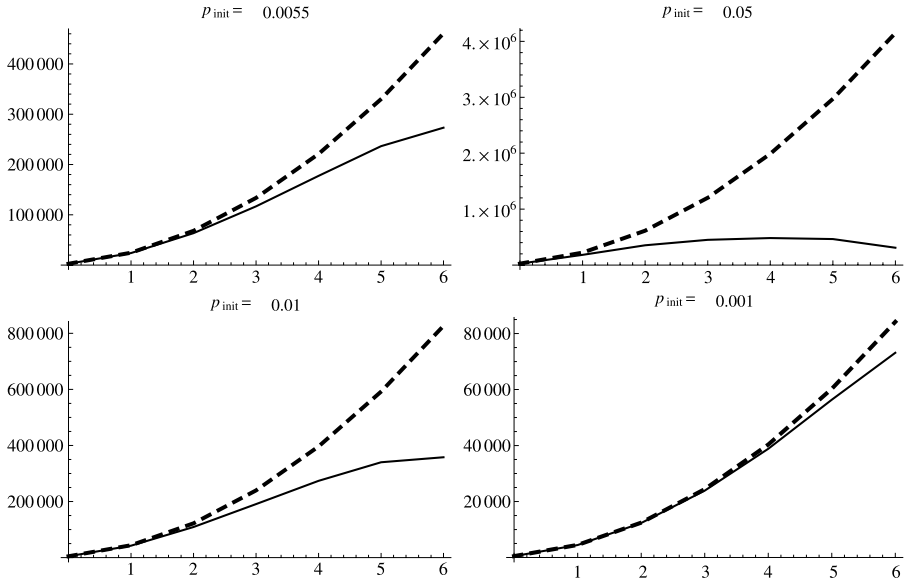


Fig. 17 Unhealthy sites in model (solid) and $k_0(2t + 1)^2$ (dashed) at t weeks in Phase 1.

precisely what leads to the Phase 2 stage, the long and frequently asymptomatic transition to AIDS.

At each subsequent time step, a larger ring of dead sites is replaced by healthy ones, and this persists for another $\tau + 2$ time steps. After a small number of additional time steps, the collisions of the squares play a large role in the dynamics and there are fewer new infections possible. Since F_1 is the most frequently occurring CA, with dead sites replaced by healthy ones, the short term behavior of the model resembles a normally operating immune system. At this stage, the dynamics are predictable to a large extent with rings of a state (1 through m) surrounded by sites at state 0. The system returns to a temporary steady state of 90% or more healthy sites as the rings of infected sites have cleared out to healthy ones which have no infected sites in their neighborhood.

The duration of the Phase 1 dynamics varies quite a bit depending on the initial viral load (the value of p_{init}); we show some typical runs in Figs. 18, 19 and 20. The output of the model agrees with clinical data (Feinberg, 2002).

Summary Given the physical constraints on τ and on the initial viral infusion into the lymph node, the Phase 1 dynamics model shows that there would be an initial drop in healthy cells, or an initial increase in unhealthy cells during the first 4 to 10 weeks, with 5–8 being most likely. If it takes k weeks to drop down to a minimum (of perhaps only 33% healthy sites), then in another k weeks most of the cells have been replenished and the lymph node is back to over 90% healthy cell sites. The entire Phase 1 cycle is over by around 20 weeks; this phase is acute infection followed by a return to at least 90% of healthy sites in the iterate of the initial point under the stochastic CA.

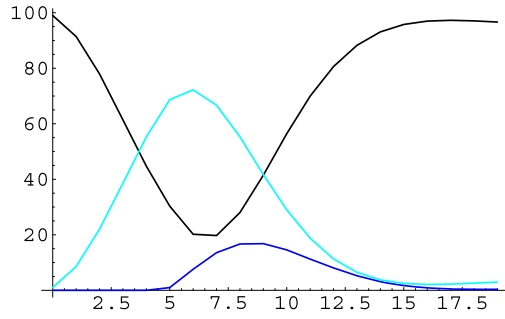


Fig. 18 Phase 1 dynamics using $p_{init} = .01$ showing % healthy (black), infected (cyan or lt. gray), and dead (blue or dk. gray) vs. weeks.

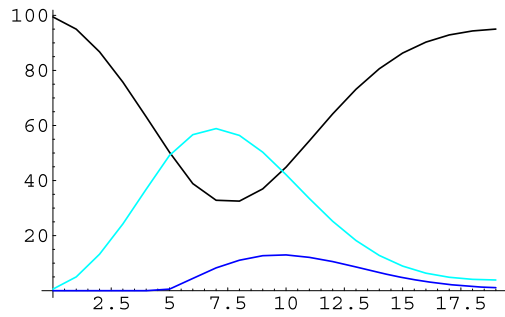


Fig. 19 Phase 1 dynamics using $p_{init} = .0055$ showing % healthy, infected, and dead vs. weeks.

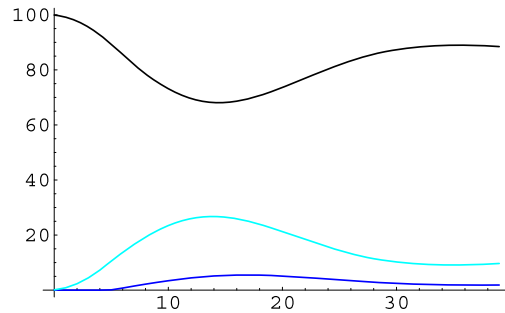


Fig. 20 Phase 1 dynamics using $p_{init} = .001$ showing % healthy, infected, and dead vs. weeks.

3.3.2. *Phase 2. Clinical latency and a gradual transition from a deterministic system to randomness*

In Phase 2, the clinical latency period, patients are observed to have a low concentration of HIV in their blood for a long time varying from 1 to 10 years; in addition, the immune system gradually deteriorates (see Fauci et al., 1996 or Nowak and May, 2000). What

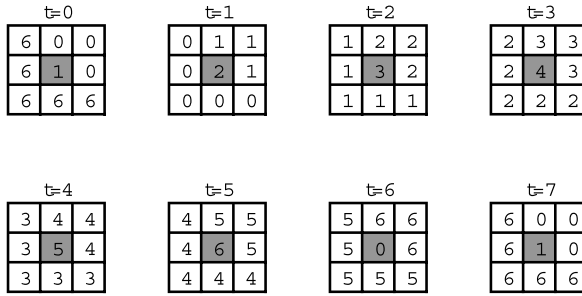


Fig. 21 The local view of a chronic source (the shaded coordinate).

we observe in the model is a slow transition from the setting of having F_1 dominate the dynamics with well-defined square or ring shaped patterns of infected sites in a backdrop of healthy sites, to the setting of Phase 3, where the configuration seems random. For an initial point x consisting of 0's with $p_{\text{init}} \cdot 100\%$ of 1's randomly distributed throughout, we see that the configurations $F_{\omega}^t(x)$ undergo a transition from a regular pattern of squares radiating out from the coordinates that were initially 1's to a point with an unpredictable neighborhood. This transition occurs for t between 12 and 18 weeks (end of Phase 1), and large values of t anywhere from 200 to 520. The squares usually remain as shadowy patterns with boundaries sprinkled with random states for large values of t .

The slow but steady increase in the number of infected and dead sites is caused by several factors. Given any point $x \in X$, we define a coordinate, x_t to be a **chronic source** if $x_t = 1$ (it is newly infected), at least r of its neighbors have value $\tau + 2$ (representing dead sites), and the rest have value 0 (healthy). This configuration arises quite naturally though rarely during the end of Phase 1 when a typical point $F_{\omega}^t(x)$ consists of many rings of 6's surrounding squares of mainly 0's as seen, for example, in the upper left box of Fig. 8. A chronic source gets its name since once formed, it generally does not disappear, but instead forms a growing square of sites containing approximately the same number of coordinates of each state, appearing in rings misshapen due to collisions. Figure 21 shows the local picture of a chronic source, and the locally periodic structure shown in Fig. 21 (compare $t = 0$ to $t = 7$) provides a clear idea of the proof of the following statement. The complete proof involves several similar cases.

Proposition 3.1. *Suppose that x_t is a chronic source, then $[F_1^{t(\tau+3)}(x)]_t = x_t$ for all $t \geq 0$.*

In the last two boxes of Fig. 16, we see the growing radius of coordinates in states other than 0 emanating from the central chronic source under the local action of f_1 . This pattern was also observed in Zorzenon dos Santos and Coutinho (2001).

An interesting feature of a chronic source is that it is created rarely, only when f_2 is the choice at precisely the moment when the defining features of a chronic source coexist (both the local geometry of the neighborhood and the probability p_2 must come together at the same time), but its continued existence depends only on the application of f_1 locally, which occurs around 99% of the time. So once created, they tend to persist as *local structures*; a chronic source could disappear under $F_{\overline{\omega}}$ by the appearance of the local rule f_3 in exactly the right spot at the right time, also a rare occurrence. The phase

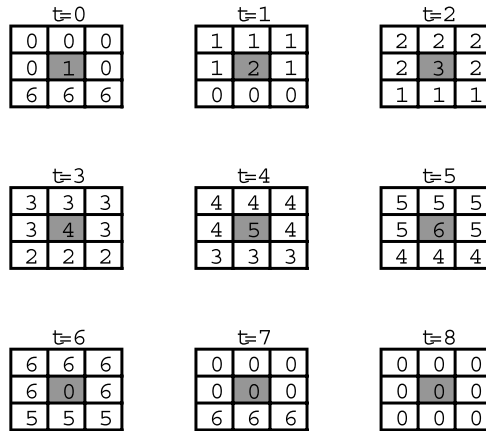


Fig. 22 The local view of an acute source (the shaded coordinate).

transition to a random field of states occurs when chronic sources collide and cover the point x over time; this takes a long time and is discussed below.

Another mathematical source of infected sites in $F_{\overline{2}}$ is a short-lived source; this type dominates the dynamics of Phase 1. If $x_t = 1$, and $r - 1$ or fewer of its neighbors have the value $\tau + 2$, while the rest have value 0, then a x_t is called an **acute source**. This structure also increases the number of infected sites, but soon clears out. It contributes in the long run to collisions and corners that fill in the areas of healthy sites. Figure 22 shows the local structure of an acute source, and the second through fourth boxes in Fig. 16 show that the interior region of zeros grows as the rings 1–6 propagate out without producing new infection. Acute sources account for the early dynamical behavior seen in Phase 1 and occur sporadically throughout Phase 2. As time passes (i.e., as t increases), there are more states in state 6 (or the final state $m = \tau + 2$), so the chance of seeing F_3 or F_2 increases with t .

One of the reasons that Phase 2 occurs and can go on for so long is that there are always opportunities for new infected sites to appear and send out acute sources of infection. This is illustrated in Fig. 22 where we show the occurrence of the local rule f_2 at a location (shaded center site) which does not cause a chronic source to form. That is, if the newly infected site is not surrounded by at least r dead sites (sites in state $\tau + 2$), then the infected sites propagate out in increasing rings, leaving a region of 0's in their interior. We note that at $t = 0$ in Fig. 22, the newly infected (shaded) site has 5 0's and 3 6's as neighbors (compare with Fig. 21). At $t = 7$, the shaded coordinate has only 3 A2 infected neighbors and will remain healthy on the 8th iteration. Except for the center coordinate, the neighborhoods shown in $t = 0$ and $t = 7$ are identical, but unless another appearance of f_2 occurs, the rings of infected sites propagate out leaving 0's in the interior (see $t = 8$). While this increases, the number of infected cells overall, under iteration of F_1 the infected cells will move away from the original site, eventually collide with other infected sites, and disappear.

The timing on the second phase This varies widely, but it is generally agreed that it is much longer—5 to 25 times longer than Phase 1; that is, if the complete acute infection

and recovery is over at 20 weeks, then it could be another 500 weeks before a patient succumbs to AIDS, 10 years after the initial infection. It can and does occur at faster scales (Feinberg, 2002; Nowak and May, 2000).

The dynamics are affected by the combination of two phenomena: the chronic sources of virus will appear with probability 1 due to the ergodic theorem (since occurrences of F_2 are almost surely going to occur), along with their relatively tiny probability that makes the time scale long and unpredictable, but the decline into Phase 3 almost inevitable.

We approximate the timing as follows. At the end of Phase 1, we estimate the percentage of chronic sources that should appear after t time steps. Using the law of large numbers, if an outcome is likely to occur with probability p_0 , $0 < p_0 < 1$, and at each of the coordinates the choice is made independently, then after one time step on the infinite grid $x \in X$ (a single point), we expect that roughly p_0 of those coordinates would produce the outcome. This simple principle drives our analysis.

We give time estimates on how long it takes to obtain enough chronic sources to cover 80% of a point $y \in X$ for points y of the form $F_{\frac{T}{\Omega}}x$, with x an allowable initial point for the model and T the time it takes to get to the end of Phase 1. At the end of Phase 1, we have about 92% of 0's and the rest of the sites are displaying in roughly equal proportions states 1–6. Of the coordinates in state 6, we need a corner coordinate in order to form a chronic source along with the choice of f_2 at the next time step. Because of collisions of squares of infected sites radiating out from the p_{init} initially infected-A1 sites, we crudely estimate that each square of 6's has perimeter around 24 with 4 of those sites being corners. So, our first constant is:

$$c = p_2 \cdot (1/6)^2 \cdot .08, \quad (19)$$

the proportion of chronic sources after 1 week. If $\chi(t)$ = proportion of chronic sources after t time steps (following the end of Phase 1), then $\chi(1) = c$.

Next, after time step k , the percentage of chronic sources is:

$$\chi(k) = \chi(k-1) + c(1 - \chi(k-1)); \quad \text{so, } \chi(k) \approx 1 - (1-c)^k. \quad (20)$$

There are two omissions in this formula: it ignores that a chronic source can be destroyed every seventh time step with a small probability (1/7 of 1%), and that chronic sources are forming expanding squares after each time step so the number of infected sites increases. However, they tend to cancel each other out in the time ranges used in the model, so we leave them out. Once we have $0 < p_0 < 1$ of the sites chronic sources, it takes around $\frac{\sqrt{(p_0^{-1})}}{2}$ time units to fill an initial point, since they form centers of growing squares.

We can look at the graph of the function which, at time t returns an estimate of time it takes to infect 80% of the sites using $\chi(t)$ chronic sources. Specifically, the graph of:

$$E(t) = t + .5\sqrt{.8}\sqrt{(\chi(t))^{-1}}$$

is shown in Fig. 23, using the largest value in the range of p_2 , 10^{-4} . The range of the function denotes the range of timing possible for the model, the shortest occurring around $t = 60$ weeks. After 60 weeks, the estimate shows that since $\chi(60) = 1.3333 \times 10^{-5}$, one

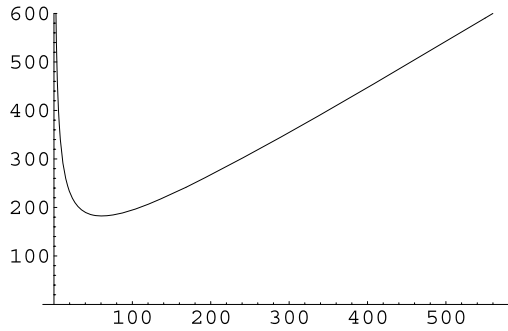


Fig. 23 Values in the range of this graph of $E(t) = t + .5\sqrt{.8}\sqrt{(\chi(t))^{-1}}$ provide estimates in weeks for Phase 2.

in every 75,000 coordinates will be a chronic source after 60 time steps; this is about one chronic source per each 274×274 square block of coordinates in y . Assuming they all persist and grow and no new ones are formed from this point on, we need to fill 80% or a block of side length 245. This will take about 122 additional time steps, bringing the total time to 182 weeks or 3.5 years. The longest time shown is about 11 years after Phase 1.

While this analysis is simplified, it gives a clear idea of the time scales involved for an initially infected point to drop down to only 20% healthy cells and it agrees with clinical findings.

3.3.3. Phase 3. The late stage of the disease and the onset of mathematical chaos

The beginning of this last stage is characterized by the loss of clear square patterns of states in a point. At this point, even though many corners of partial squares are visible, given a coordinate x_i there is no way of predicting what states will be in its immediate neighborhood; indeed, it is somewhat random. At this stage, the dynamics are acting like a zero radius Markov process, acting independently at each coordinate with probability transitions determined by the local rules f_1 , f_2 , and f_3 .

Using the probabilities from p along with the CA rules, one can form a stochastic matrix Q , whose left eigenvector q shows an essentially (but not quite) equal distribution among the 7 states. This then leads to only about 14% (or a slightly different percentage depending on the value of τ) of the cells remaining healthy and by this time there is essentially no return to Phase 1 dynamics. (Actually it remains a mathematical possibility with a very tiny probability of occurring and no estimate on the timing of the return.) In Section 5, we prove that with probability 1 we reach this “point of no return.” More details of this last phase of the model are explained in Section 5.

While the onset of Phase 3 dynamics is often at or about the time of the onset of AIDS, it is important to understand mathematically what is going on at this time since the system is heading in this direction for many weeks leading up to its onset. In other words, the Phase 3 behavior of the model may have no clinical analog (an individual is unlikely to survive very far into this stage), but is of great mathematical importance as later theorems will indicate that it represents a dynamical equilibrium towards which the model lymph node is heading for many years.

4. Dynamical properties of the CA's in the model

In this section, we give a mathematical analysis of the CAs used in the model, both individually and taken as a stochastic CA. We begin this by proving some results about the individual cellular automata used in the model $F_{\bar{0}}$; results are stated using $\tau = 4$, so we have an alphabet with 7 states, but are true for any value of τ within the range given in Zorzenon dos Santos and Coutinho (2001) without any changes. We also use $r = 4$ in the analysis here. Most of the results hold for any value of r within the range specified in Zorzenon dos Santos and Coutinho (2001) without any changes; we state explicitly where $r = 4$ is needed.

Let the state space be $A = \{0, 1, \dots, 6\}$ and recall the three local rules $f_1, f_2, f_3 : A^{3 \times 3} \rightarrow A$:

$$f_1, f_2, f_3 \left(\begin{array}{ccc} * & * & * \\ * & 0 & * \\ * & * & * \end{array} \right) = \begin{cases} 1 & \text{if } \geq 1 \text{ * is } 1, 2, 3, \text{ or } 4, \text{ or if } \geq 4 \text{ *'s are } 5\text{'s} \\ 0 & \text{otherwise,} \end{cases}$$

$$f_1, f_2, f_3 \left(\begin{array}{ccc} * & * & * \\ * & a & * \\ * & * & * \end{array} \right) = a + 1 \quad \text{for } 1 \leq a \leq 5,$$

$$f_1 \left(\begin{array}{ccc} * & * & * \\ * & 6 & * \\ * & * & * \end{array} \right) = 0, \quad f_2 \left(\begin{array}{ccc} * & * & * \\ * & 6 & * \\ * & * & * \end{array} \right) = 1, \quad f_3 \left(\begin{array}{ccc} * & * & * \\ * & 6 & * \\ * & * & * \end{array} \right) = 6.$$

Denote by $F_1, F_2, F_3 : \mathcal{A}^{\mathbb{Z}^2} \rightarrow \mathcal{A}^{\mathbb{Z}^2}$ the CA with local rule f_1, f_2, f_3 , respectively. These are the CAs of the HIV model in Zorzenon dos Santos and Coutinho (2001). Let $\bar{0} \in \mathcal{A}^{\mathbb{Z}^2}$ be the point having each coordinate $\bar{0}_{(i_1, i_2)} = 0$ for all $i_1, i_2 \in \mathbb{Z}$ and similarly, let $\bar{6} \in \mathcal{A}^{\mathbb{Z}^2}$ be such that $\bar{6}_{(i_1, i_2)} = 6$ for all $i_1, i_2 \in \mathbb{Z}$.

The first result in this section says that there exist points arbitrarily close to the ‘‘all healthy’’ configuration such that, under iteration of any one of the three rules individually, the trajectories of the two points will be fundamentally different at some point in time.

Proposition 4.1. *The point $\bar{0}$ is not a point of equicontinuity for F_1, F_2 , or F_3 .*

Proof: Let $\varepsilon = 1$, and let $\delta = 2^{-L} > 0$. We choose x with $d_X(x, \bar{0}) < \delta$ so that $x_{(0, L+1)} = 1$ and $x_{(i_1, i_2)} = 0$ for all $(i_1, i_2) \in \mathbb{Z}^2 \setminus \{(0, L+1)\}$. Notice that $\bar{0}$ is a fixed point under each of the CAs, F_1, F_2 , and F_3 . However, $F_j^{L+1}x$ has a 1 at the position $(0, 0)$ for $j \in \{1, 2, 3\}$, and so $d_X(F_j^{L+1}x, F_j^{L+1}\bar{0}) = 1 \not< \varepsilon$. Thus, for $\varepsilon = 1$, there is no δ which satisfies the equicontinuity definition, and so $\bar{0}$ is not a point of equicontinuity for any of these three CAs. \square

We next analyze the behavior of initial points drawn from those considered in the original model under iteration of F_1, F_2 , and F_3 individually. These points consist of the values 0 and 1 only. We study the orbits of such points and the question of whether these are points of equicontinuity in Propositions 4.3, 4.4, 4.5, and 4.7. In the proofs of each of these, we begin in essentially the same manner: for a point consisting only of 0's and 1's,

we look for the 1 closest to a central neighborhood and determine how long it takes for this value to propagate through the given central region. Therefore, we first approach this common idea with Lemma 4.2.

This result supports the observation that if we define a **healthy block** to be an $L \times L$ block of 0's located somewhere in a point x , eventually every healthy block will be filled in with infection as $F_{\bar{w}}$ is applied, no matter which $\bar{w} \in \bar{\mathcal{O}}$ is used. Another way to phrase the next lemma is to say that no healthy blocks persist under the action of this HIV model.

Lemma 4.2. *Let $x \in \mathcal{A}^{\mathbb{Z}^2}$ have $x_{(i_1, i_2)} \in \{0, 1\}$ for all $i_1, i_2 \in \mathbb{Z}$, but $x \neq \bar{0}$. Given an integer $k > 0$, let $N_k = \{(i_1, i_2) : |i_1|, |i_2| \leq k\} \subseteq \mathbb{Z}^2$ be the neighborhood of radius k about $\bar{0} \in \mathbb{Z}^2$, and let $T = \min\{\|(m_1, m_2) - N_k\| : x_{(m_1, m_2)} = 1\}$ be the minimum distance a value 1 is to the neighborhood N_k . Then for each $(i_1, i_2) \in N_k$ and each $j \in \{1, 2, 3\}$, $(F_j^t x)_{(i_1, i_2)} = 1$ for some $t \leq T + 2k$.*

Proof: Let x , k , N_k , and T be as in the statement of the lemma. Further, let $(M_1, M_2) \in \mathbb{Z}^2$ be a pair satisfying $\|(M_1, M_2) - N_k\| = T$. If $T = 0$, we can take (M_1, M_2) to be the position closest to the origin where x has a 1. That is, T tells how many steps away from the neighborhood N_k a value 1 is, and (M_1, M_2) is the index pair for this closest 1 (the closest such position to the origin if $T = 0$). Now, only a value 0 at time t which is adjacent to a value 1 will update to the value 1 at time $t + 1$ under F_1 , F_2 , or F_3 . Therefore, under iteration of F_j , $j \in \{1, 2, 3\}$, 1 values propagate through a group of 0 values at a constant rate of one position per time step in each of the eight directions, and so it will take T time steps for the 1 at (M_1, M_2) to propagate into the neighborhood N_k . That is, $[F_j^T(x)]_{(i_1, i_2)} = 1$ for some $(i_1, i_2) \in N_k$ and for each $j \in \{1, 2, 3\}$. Then as the neighborhood N_k has length and width $2k + 1$, it will take at most $2k$ time steps more for every index pair of N_k to have taken on the value 1. Thus, for each $(i_1, i_2) \in N_k$ and each $j \in \{1, 2, 3\}$, $(F_j^t x)_{(i_1, i_2)} = 1$ for some $t \leq T + 2k$. \square

The next result shows that F_1 , the dominant CA in the model, occurring around 99% of the time, reflects a working immune system under an ordinary viral infection. More precisely, we show in Proposition 4.3 that initial points consisting of 0's and 1's converge to the point having all values 0 (a completely healthy lymph node) under iteration of F_1 . The orbit of such an initial point, acted on by F_1 , is shown in Fig. 24.

Proposition 4.3. *If $x \in \mathcal{A}^{\mathbb{Z}^2}$ has $x_{(i_1, i_2)} \in \{0, 1\}$ for all $i_1, i_2 \in \mathbb{Z}$, then*

$$\lim_{t \rightarrow \infty} F_1^t(x) = \bar{0}.$$

Proof: Let $x \in \mathcal{A}^{\mathbb{Z}^2}$ have $x_{(i_1, i_2)} \in \{0, 1\}$ for all $i_1, i_2 \in \mathbb{Z}$, let $\varepsilon = 2^{-k} > 0$, and let $N_k = \{(i_1, i_2) \in \mathbb{Z}^2 : |i_1|, |i_2| \leq k\}$ be the neighborhood with radius k about $\bar{0} \in \mathbb{Z}^2$. Since $\bar{0}$ is a fixed point for F_1 , let us assume that there exists at least one pair $(m_1, m_2) \in \mathbb{Z}^2$ so that $x_{(m_1, m_2)} = 1$. As in Lemma 4.2, let $T = \min\{\|(m_1, m_2) - N_k\| : x_{(m_1, m_2)} = 1\}$, so that by at most $T + 2k$ time steps, each coordinate of x with index in N_k has become 1. Once a coordinate takes on the value 1, it will pass through states 2, 3, 4, 5, 6, and 0 in the successive 6 time steps. Thus, after $T' = T + 2k + 6$ time steps, each coordinate $x_{(i_1, i_2)}$ with $(i_1, i_2) \in N_k$ has become 0. These coordinates will then remain 0, since between

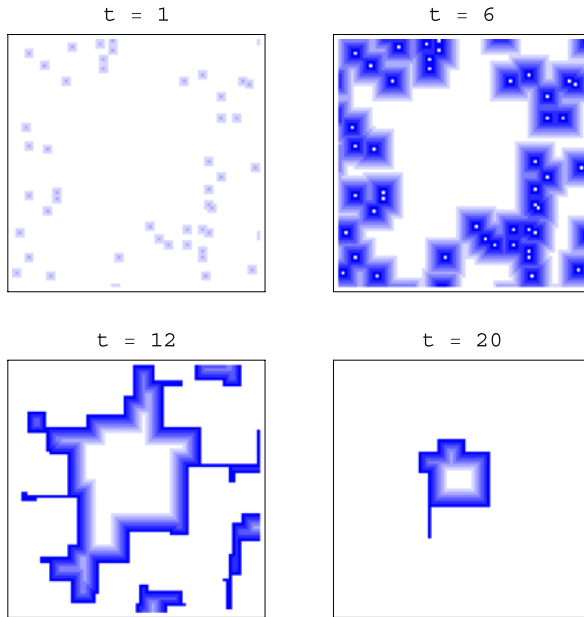


Fig. 24 Iterates F_1x , F_1^6x , $F_1^{12}x$, and $F_1^{20}x$ where $x_{(i_1, i_2)} \in \{0, 1\}$, $i_1, i_2 \in \mathbb{Z}$ progressing to a central block of 0's.

any 0 within N_k and any 1 outside N_k , there is at least one band of consecutive values 1–2–3–4–5–6, and by this time, the value 0 can only be adjacent to other 0's and/or 6's. Therefore, for $t \geq T'$, $(F_1^t x)_{(i_1, i_2)} = 0$ for $(i_1, i_2) \in N_k$, or $d_X(F_1^t x, \bar{0}) < \varepsilon$ for $t \geq T'$, and so $\lim_{t \rightarrow \infty} F_1^t x = \bar{0}$, as desired. \square

Although there is no biological basis known to the authors for considering the action of F_3 on its own, it is mathematically interesting to make parallel statements to those we have for F_1 . Under iteration of only F_3 , initial points from Zorzenon dos Santos and Coutinho (2001) converge to the point consisting entirely of 6's (a completely “dead” lymph node). The orbit under F_3 for such an initial point is shown in Fig. 25.

Proposition 4.4. *If $x \in \mathcal{A}^{\mathbb{Z}^2}$ has $x_{(i_1, i_2)} \in \{0, 1\}$ for all $i_1, i_2 \in \mathbb{Z}$ and $x \neq \bar{0}$, then*

$$\lim_{t \rightarrow \infty} F_3^t(x) = \bar{6}.$$

Proof: Let $x \in \mathcal{A}^{\mathbb{Z}^2} \setminus \{\bar{0}\}$ have $x_{(i_1, i_2)} \in \{0, 1\}$ for all $i_1, i_2 \in \mathbb{Z}$, let $\varepsilon = 2^{-k} > 0$, and let $N_k = \{(i_1, i_2) \in \mathbb{Z}^2 : |i_1|, |i_2| \leq k\}$ be the neighborhood with radius k about $\bar{0} \in \mathbb{Z}^2$. As in Lemma 4.2, let $T = \min\{\|(m_1, m_2) - N_k\| : x_{(m_1, m_2)} = 1\}$, so that by at most $T + 2k$ time steps, each coordinate of x with index in N_k has become 1. Once a coordinate takes on the value 1, it will pass through states 2, 3, 4, 5, and 6 in the successive 5 time steps. Under F_3 , a 6 remains a 6. Thus, after $T' = T + 2k + 5$ time steps, each coordinate $x_{(i_1, i_2)}$ with $(i_1, i_2) \in N_k$ has become 6 and will stay 6 for all time. Therefore, for $t \geq T'$,

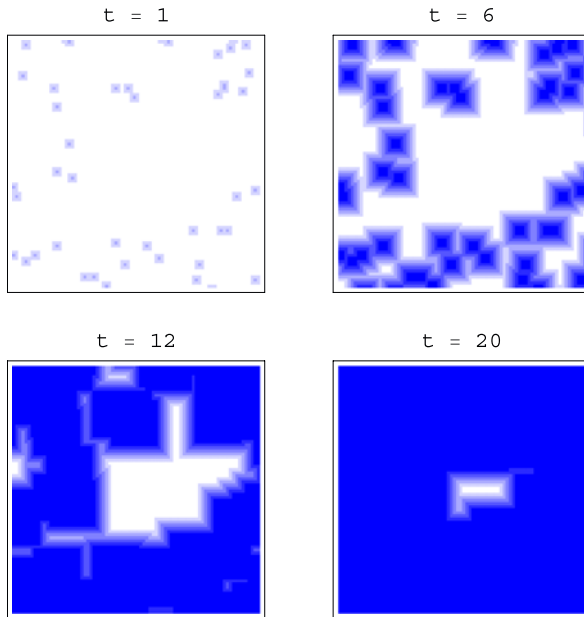


Fig. 25 Iterates F_3x , F_3^6x , $F_3^{12}x$, and $F_3^{20}x$ where $x_{(i_1,i_2)} \in \{0, 1\}$, $i_1, i_2 \in \mathbb{Z}$ progressing to a central of block $\bar{6}$'s.

$(F_3^t x)_{(i_1,i_2)} = 6$ for $(i_1, i_2) \in N_k$, or $d_X(F_3^t x, \bar{6}) < \varepsilon$ for $t \geq T'$, and so $\{F_3^t x\}_{t \geq 0} \rightarrow \bar{6}$, as desired. \square

Under F_2 , where the value 6 is mapped to 1, initial points consisting of all 0's and 1's—those considered by the model of Zorzenon dos Santos and Coutinho (2001)—tend to a periodic orbit where each coordinate cycles through the values 1–6. A typical orbit for such an initial point is shown in Fig. 26. It is the presence of the rule F_2 in the stochastic CA which is central to the appearance of chronic sources, since it causes an interruption to the regular bands of 1–2–3–4–5–6–0 which form under application of F_1 .

Although initial points consisting of only 0's and 1's converge to a fixed point under both F_1 and F_3 , we see that nearby points in the metric topology do not behave similarly with respect to these two CAs. Under F_1 , the points consisting of 0's and 1's are not points of equicontinuity (Proposition 4.7); however, they are equicontinuity points for both F_2 and F_3 (Proposition 4.5). That is to say, knowing only that we have a point which is very close to an initial point coming from Zorzenon dos Santos and Coutinho (2001) is good enough to predict the orbit under just F_2 or just F_3 , but not good enough to predict the orbit under F_1 .

The idea of the proofs for F_2 and F_3 is that once a coordinate has taken on the value 1, that coordinate's values are determined for all time: 1, 2, 3, 4, 5, 6, 1, 2, 3, 4, 5, 6, etc. for F_2 and 1, 2, 3, 4, 5, 6, 6, 6, 6, etc. for F_3 . So, given an ε and initial x , we choose δ small enough using Lemma 4.2 so that the propagation of a 1 through the epsilon region takes places before any far away differences in x and any v within δ of x can enter this zone. Under F_1 , however, the introduction of the value 1 to a site does not predetermine what

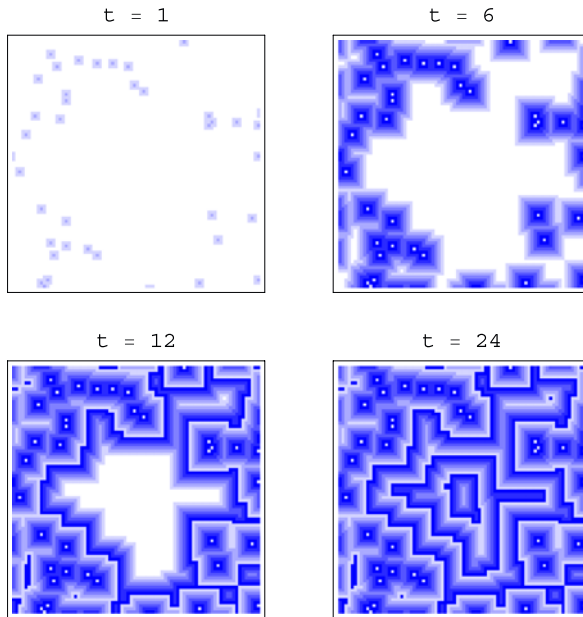


Fig. 26 Iterates F_2x , F_2^6x , $F_2^{12}x$, and $F_2^{24}x$ where $x_{(i_1, i_2)} \in \{0, 1\}$, $i_1, i_2 \in \mathbb{Z}$. Here, $F_2^{24}x$ is periodic with period 6.

value that site will take on for all time, and so we can find points close to any initial point of 0's and 1's whose orbits do not stay close to that of our given point for all time. We hold off on the proof for F_1 for now.

Proposition 4.5. *If $x \in \mathcal{A}^{\mathbb{Z}^2}$ has $x_{(i_1, i_2)} \in \{0, 1\}$ for all $i_1, i_2 \in \mathbb{Z}$ but $x \neq \bar{0}$, then x is a point of equicontinuity under F_2 and F_3 .*

Proof: Let x be as in the statement of the proposition, let $\varepsilon = 2^{-k} > 0$, and let N_k and T be as in Lemma 4.2. Thus, for each $(i_1, i_2) \in N_k$ and $j \in \{2, 3\}$, $(F_j^t x)_{(i_1, i_2)} = 1$ for some $t \leq T + 2k$. Then $(F_j^t x)_{(i_1, i_2)}$ will be determined for all $(i_1, i_2) \in N_k$ for $t > T + 2k$, $j \in \{2, 3\}$. Let $L = k + (T + 2k)$ and let $\delta = 2^{-L}$. Now for any v with $d_X(x, v) < \delta$, we know that the values of $[F_j^t(v)]_{N_k}$ and $[F_j^t(x)]_{N_k}$ will have entered their (same) determined cycle when $t = T + 2k$ and so any difference v has from x cannot influence the values in the neighborhood N_k during this time, by our choice of L . Thus, x is a point of equicontinuity for both F_2 and F_3 . \square

The next lemma says that while there is great unpredictability in what happens to healthy blocks, there are other blocks which have a completely predictable orbit under each one of the rules F_1, F_2, F_3 . For this lemma, we require that $r \leq 5$ in the case of F_1 ; for the cases F_2 and F_3 , the proof holds for any $2 \leq r \leq 8$.

Lemma 4.6. *For $2 \leq r \leq 5$, every pattern consisting of a square ring of 2's between two contiguous square rings of 0's, i.e., of the form of (21), is a fully blocking pattern under each F_j , $j \in \{1, 2, 3\}$. Further, these patterns are fully blocking patterns under F_j , $j \in \{2, 3\}$ for $2 \leq r \leq 8$.*

$$\begin{array}{cccccccc}
 0 & \dots & \dots & \dots & 0 & \dots & \dots & \dots & 0 \\
 \vdots & 2 & \dots & \dots & 2 & \dots & \dots & 2 & \vdots \\
 \vdots & \vdots & 0 & \dots & 0 & \dots & 0 & \vdots & \vdots \\
 \vdots & \vdots & \vdots & & & & \vdots & \vdots & \vdots \\
 0 & 2 & 0 & & & & 0 & 2 & 0 \\
 \vdots & \vdots & \vdots & & & & \vdots & \vdots & \vdots \\
 \vdots & \vdots & 0 & \dots & 0 & \dots & 0 & \vdots & \vdots \\
 \vdots & 2 & \dots & \dots & 2 & \dots & \dots & 2 & \vdots \\
 0 & \dots & \dots & \dots & 0 & \dots & \dots & \dots & 0
 \end{array} \tag{21}$$

Proof: Let $x \in \mathcal{A}^{\mathbb{Z}^2}$ be a point in which the above pattern appears. To fix the position of the pattern, let $l > 0$ and let

$$R_l = \{(i_1, i_2) \in \mathbb{Z}^2 : |i| = l, |j| \leq l \text{ or } |i| \leq l, |j| = l\} \tag{22}$$

be a ring of indices of \mathbb{Z}^2 where x takes on the value 2. Similarly, let R_{l-1} and R_{l+1} be defined to be the rings of indices of \mathbb{Z}^2 adjacent to R_l to the interior and to the exterior, respectively, where all coordinates of x in R_{l-1} and R_{l+1} have the value 0. So for each $(i_1, i_2) \in R_{l-1} \cup R_{l+1}$, $x_{(i_1, i_2)} = 0$ and is adjacent to at least one value 2. Thus, $(F_j x)_{(i_1, i_2)}$ has the value 1 for $(i_1, i_2) \in R_{l-1} \cup R_{l+1}$ and has the value 3 for $(i_1, i_2) \in R_l$, for each $j \in \{1, 2, 3\}$. As we iterate F_j further, these values cycle through the sequence 1–2–3–4 in $R_{l-1} \cup R_{l+1}$ and through 3–4–5–6 in R_l . At this point, we must break into the different cases for j .

Taking one more iteration of F_1 , we see that $(F_1^5 x)_{(i_1, i_2)}$ has the value 5 for $(i_1, i_2) \in R_{l-1} \cup R_{l+1}$ and the value 0 for $(i_1, i_2) \in R_l$. Now, all the 0's in R_l are adjacent to two 0's and either five or six 5's, so that $(F_1^6 x)_{(i_1, i_2)} = 1$ for $(i_1, i_2) \in R_l$, provided that $2 \leq r \leq 6$, and $(F_1^6 x)_{(i_1, i_2)} = 6$ for $(i_1, i_2) \in R_{l-1} \cup R_{l+1}$. Then $(F_1^7 x)_{(i_1, i_2)} = 2$ for $(i_1, i_2) \in R_l$ and $(F_1^7 x)_{(i_1, i_2)} = 0$ for $(i_1, i_2) \in R_{l-1} \cup R_{l+1}$; we're back to the situation we had at the indices of $R_{l-1} \cup R_l \cup R_{l+1}$ for x itself. Thus, the pattern of (21) is periodic with period 7 under F_1 .

We know $(F_2^4 x)_{(i_1, i_2)}$ takes on the value 4 at indices $(i_1, i_2) \in R_{l-1} \cup R_{l+1}$ and the value 6 at indices $(i_1, i_2) \in R_l$; we follow these patterns under further iteration of F_2 . So, $(F_2^5 x)|_{R_{l-1} \cup R_{l+1}} = 5$ and $(F_2^5 x)|_{R_l} = 1$, $(F_2^6 x)|_{R_{l-1} \cup R_{l+1}} = 6$ and $(F_2^6 x)|_{R_l} = 2$, and finally $(F_2^7 x)|_{R_{l-1} \cup R_{l+1}} = 1$ and $(F_2^7 x)|_{R_l} = 3$. This is the situation of $(F_2 x)|_{R_{l-1} \cup R_l \cup R_{l+1}}$. Therefore, the pattern of (21) is eventually periodic under F_2 with pre-period 1 and period 6. The values here are independent of the value of r .

Similarly, the coordinates $(F_3^4 x)_{(i_1, i_2)}$ have the value 4 for $(i_1, i_2) \in R_{l-1} \cup R_{l+1}$ and the value 6 for $(i_1, i_2) \in R_l$. Continuing iteration of F_3 gives $(F_3^5 x)|_{R_{l-1} \cup R_{l+1}} = 5$ and

$(F_3^5 x)|_{R_l} = 6$, and then $(F_3^6 x)|_{R_{l-1} \cup R_l \cup R_{l+1}} = 6$. So, the pattern of (21) is eventually fixed under F_3 with preperiod 6. Again, the values here are independent of the value of r .

Since each of these progressions of values depends only on the values of $x|_{R_{l-1} \cup R_l \cup R_{l+1}}$ and no other values of x , every pattern of the form of (21) is a fully blocking pattern for each F_j , $j \in \{1, 2, 3\}$. \square

Now we are ready to prove that although F_1 , which models the fully functioning immune system, is used close to 99% of the time, even this rule is unpredictable. Since the next proof utilizes Lemma 4.6, we require $2 \leq r \leq 5$ here as well.

Proposition 4.7. *If $x \in \mathcal{A}^{\mathbb{Z}^2}$ has $x_{(i_1, i_2)} \in \{0, 1\}$ for all $i_1, i_2 \in \mathbb{Z}$, then x is not a point of equicontinuity for F_1 .*

Proof: Let x be as in the statement of the proposition, take $\varepsilon = 2^{-k} > 0$, and let $\delta = 2^{-L} > 0$. Let N_k be the neighborhood with radius k of $\vec{0} \in \mathbb{Z}^2$, and as in Lemma 4.2, let (M_1, M_2) be the coordinates of \mathbb{Z}^2 closest to N_k such that $x_{(M_1, M_2)} = 1$, and let T be the distance between (M_1, M_2) and N_k . We may assume that $\delta \leq \varepsilon$, so that $L \geq k$. In order to produce a point $v \in \mathcal{A}^{\mathbb{Z}^2}$ contradicting the definition for x to be a point of equicontinuity for F_1 , we break into two cases, where $T > L - k$ or $T \leq L - k$.

If $T > L - k$, then the coordinates $x_{(i_1, i_2)} = 0$ for $(i_1, i_2) \in N_k$. Choose $v = \vec{0}$; thus, $d_X(x, v) < \delta$. As $\vec{0}$ is fixed for F_1 , the coordinates $[F_1^t(\vec{0})]_{(i_1, i_2)} = 0$ for $(i_1, i_2) \in N_k$ and for all iterates $t \geq 0$. However, by time $T + 1$, the 1 at position (M_1, M_2) of x will have propagated into the neighborhood N_k . Therefore, $d_X(F_1^{T+1}x, F_1^{T+1}\vec{0}) \geq \varepsilon$, and so x is not a point of equicontinuity for F_1 .

If $T \leq L - k$, we choose v with $d_X(x, v) < \delta$ in the following way. Take $v_{(i_1, i_2)} = x_{(i_1, i_2)}$ for $|i|, |j| \leq L$, take $v_{(i_1, i_2)} = 2$ for $|i| = L + 2$, $|j| \leq L + 2$ and $|i| \leq L + 2$, $|j| = L + 2$, and take $v_{(i_1, i_2)} = 0$ for all other pairs $(i_1, i_2) \in \mathbb{Z}^2$. That is, v agrees with x on the neighborhood of radius L about $\vec{0} \in \mathbb{Z}^2$, v has a ring of 0's around this neighborhood, a ring of 2's around that neighborhood, and has 0's outside of the central $(2L + 5) \times (2L + 5)$ region. Recall that by Proposition 4.3, there exists $T_1 = T + 2k + 6 > 0$ such that for $t \geq T_1$, $(F_1^t x)|_{(i_1, i_2)} = 0$ for $(i_1, i_2) \in N_k$.

Taking $l = L + 2$, we have that $v|_{R_{l-1} \cup R_l \cup R_{l+1}}$ is a fully blocking pattern as in Proposition 4.6. Let us investigate what happens to the coordinates v_{N_k} under iteration of F_1 . Since $T \leq L - k$, $v_{(M_1, M_2)} = 1$ and the initial 2's in v are a distance of $L + 2 - k \geq T + 2$ from the neighborhood N_k . It will take $\lfloor \frac{L+2-T}{2} \rfloor$ steps until the 1 at (M_1, M_2) and an initial 2 at a position in R_{L+2} have propagated an infected value of 1, 2, 3, or 4 to adjacent positions between R_{L+2} and (M_1, M_2) . Then it will take 6 more steps for the 1 propagated from (M_1, M_2) to cycle through the values 2–3–4–5–6–0. At this point, there are only values of 0 between the infected value originating from R_{L+2} and N_k . Thus, it can take at most $L + 2$ more iterations until this infected cell propagates to the neighborhood N_k . Let $T_2 = \lfloor \frac{L+2-T}{2} \rfloor + 6 + L + 2$. Since the coordinates $v_{R_{L+1} \cup R_{L+2} \cup R_{L+3}}$ continue to propagate infected values through a group of 0's for all time, then there exists $T' \geq \max\{T_1, T_2\}$ such that $(F_1^{T'} v)|_{(i_1, i_2)} \neq 0$ for some pair $(i_1, i_2) \in N_k$. Therefore, $d_X(F_1^{T'} x, F_1^{T'} v) \geq \varepsilon$, and so x is not a point of equicontinuity for F_1 . \square

We next show that there are many initial points in $\mathcal{A}^{\mathbb{Z}^2}$ (forming a dense G_δ set) that do have predictable trajectories under each of the rules F_1, F_2, F_3 when applied alone.

We use the blocks of Lemma 4.6 to obtain such initial conditions. Therefore, the next proposition holds for F_1 when $2 \leq r \leq 5$, and for F_2 and F_3 in all cases ($2 \leq r \leq 8$).

Proposition 4.8. F_j is almost equicontinuous for $j \in \{1, 2, 3\}$.

Proof: By Lemma 4.6, the pattern

$$\begin{array}{cccccc} 0 & 0 & 0 & 0 & 0 & 0 & 0 \\ 0 & 2 & 2 & 2 & 2 & 2 & 0 \\ 0 & 2 & 0 & 0 & 0 & 2 & 0 \\ 0 & 2 & 0 & 0 & 0 & 2 & 0 \\ 0 & 2 & 0 & 0 & 0 & 2 & 0 \\ 0 & 2 & 2 & 2 & 2 & 2 & 0 \\ 0 & 0 & 0 & 0 & 0 & 0 & 0 \end{array}$$

is fully blocking for each F_j , $j \in \{1, 2, 3\}$. Thus, by Proposition 2.9, F_j is almost equicontinuous for $j \in \{1, 2, 3\}$. \square

Lemma 4.6 provides us with a pattern which is fully blocking under each of the rules F_1 , F_2 , and F_3 individually. However, it is important to note that the sequence of iterates of the blocking pattern is not the same under each of the three rules, and so we cannot invoke Theorem 2.11 to guarantee points of equicontinuity in the stochastic CA. In fact, there are no such points in $F_{\bar{\omega}}$ for any choice of $\bar{\omega} \in \bar{\Omega}$; this is the content of the next theorem.

Theorem 4.9. *The stochastic CA generated by F_1 , F_2 , and F_3 does not have any points of equicontinuity.*

Proof: Let $\varepsilon = 1$, and $\delta = 2^{-M}$. We show that for any $y \in Y$, $y_{\bar{t}} = (\omega^{(\bar{t})}, x_{\bar{t}})$, there exists $z \in Y$, $z_{\bar{t}} = (\zeta^{(\bar{t})}, v_{\bar{t}})$ and t^* such that $\rho(y, z) < \delta$ and $d_X(F_{\bar{\omega}}^{t^*} x, F_{\bar{\zeta}}^{t^*} v) \geq \varepsilon$, where the points $x, v \in X$ and $\bar{\omega}, \bar{\zeta} \in \bar{\Omega}$ are obtained from v and z in the canonical way. Therefore, v is not a point of equicontinuity for \bar{F} , and hence no x is a point of equicontinuity for the stochastic CA $F_{\bar{\Omega}}$. For simplicity, we write $v = (\bar{\omega}, x)$ and $z = (\bar{\zeta}, v)$.

First, suppose that $y = (\bar{\omega}, x)$ is such that $F_{\bar{\omega}}^t x$ follows the typical progression that we observe in simulations. That is, after some time, each coordinate $[F_{\bar{\omega}}^t x]_{\bar{t}}$ cycles through the values 0, 1, 2, 3, 4, 5, and 6, possibly with some hesitations ($6 \rightarrow 6$ for one or more time steps) and possibly with some skips ($6 \rightarrow 1$ at some time step). Let $v = x$, and define $\bar{\zeta}$ by $\zeta^{(\bar{t})} = \omega^{(\bar{t})}$ for $\bar{t} \neq (0, 0)$, $\zeta_j^{(0,0)} = \omega_j^{(0,0)}$ for $j \leq M$, and $\zeta_j^{(0,0)} = 3$ for $j > M$. Now let $z = (\bar{\zeta}, v)$; clearly $\rho(v, z) < \delta$.

The central coordinate, $[F_{\bar{\zeta}}^t v]_{(0,0)}$, will follow the progression of $[F_{\bar{\omega}}^t x]_{(0,0)}$ at least until time $t = M$, and possibly longer, until for some time $T > M$, $[F_{\bar{\omega}}^T x]_{(0,0)} = [F_{\bar{\zeta}}^T v]_{(0,0)} = 6$. Then for all $t \geq T$, $[F_{\bar{\zeta}}^t v]_{(0,0)} = 6$ by construction of $\zeta^{(0,0)}$. However, by the assumption on v , there is some time T' beyond which $[F_{\bar{\omega}}^t x]_{(0,0)}$ cycles through the values 0, 1, 2, 3, 4, 5, and 6, possibly with some hesitations and possibly with some skips, so that there exists $t^* \geq \max\{T, T'\}$ such that $[F_{\bar{\omega}}^{t^*} x]_{(0,0)} \neq 6$. Thus, $d_X(F_{\bar{\omega}}^{t^*} x, F_{\bar{\zeta}}^{t^*} v) = 1$, and so

$d_X(\{[F_{\bar{\omega}}^{t*}x]_{\vec{r}}\}_{\vec{r} \in \mathbb{Z}^2}, \{[F_{\bar{\zeta}}^{t*}v]_{\vec{r}}\}_{\vec{r} \in \mathbb{Z}^2}) \geq 1$. Therefore, v is not a point of equicontinuity for \bar{F} , and so x is not a point of equicontinuity for $F_{\bar{\omega}}$.

The proof above works for any $y = (\bar{\omega}, x)$ with the property that given any $T > M$, there exists $T' \geq T$ such that $[F_{\bar{\omega}}^{T'}x]_{(0,0)} \neq 6$. Now suppose that $y = (\bar{\omega}, x)$ does not have this property, i.e. $[F_{\bar{\omega}}^t x]_{(0,0)} = 6$ for all $t > M$. Then it must be the case that $[F_{\bar{\omega}}^{M+1}x]_{(0,0)} = 6$ and $\omega_j^{(0,0)} = 3$ for all $j > M$. In order to show that this y is not a point of equicontinuity for \bar{F} either, let $v = x$, let $\zeta^{(\vec{r})} = \omega^{(\vec{r})}$ for $\vec{r} \neq (0, 0)$, let $\zeta_j^{(0,0)} = \omega_j^{(0,0)}$ for $j \leq M$, and let $\zeta_j^{(0,0)} = 1$ for all $j > M$. Again, let $z = (\bar{\zeta}, v)$; it is clear that $\rho(y, z) < \delta$.

As in the previous case, the coordinates $[F_{\bar{\zeta}}^t v]_{(0,0)}$ and $[F_{\bar{\omega}}^t x]_{(0,0)}$ will follow the same progression until time $t = M + 1$. Thus, $[F_{\bar{\zeta}}^{M+1}v]_{(0,0)} = 6$ and since $\zeta_{M+1}^{(0,0)} = 1$, we have $[F_{\bar{\zeta}}^{M+2}v]_{(0,0)} = 0$. However, we also have $[F_{\bar{\omega}}^{M+2}x]_{(0,0)} = 6$, and so $d_X(\{[F_{\bar{\omega}}^{M+2}x]_{\vec{r}}\}_{\vec{r} \in \mathbb{Z}^2}, \{[F_{\bar{\zeta}}^{M+2}v]_{\vec{r}}\}_{\vec{r} \in \mathbb{Z}^2}) \geq 1$. Therefore, y is not a point of equicontinuity for \bar{F} , and so x is not a point of equicontinuity for $F_{\bar{\omega}}$, as desired. \square

5. Phase three of the HIV virus dynamics: a Markov CA

In Phase 3, when the onset of AIDS occurs, a patient's immune system is compromised by virtue of having 20% or less of the normal number of CD4⁺ T-cells remaining. This often causes opportunistic infections to lead to the death of the patient (see e.g. Pantaleo and Fauci, 1996, p. 849). This phase in the mathematical model is characterized by the following property: for each $x \in X$, and any coordinate $x_{(i,j)}$ of x , the values in a neighborhood of $x_{(i,j)}$ are unpredictable and appear more random than deterministic. In fact, if the model is allowed to run indefinitely, mathematically the system usually settles down to a Markov chain. In what follows, we show that the Markov behavior usually appears somewhat after the percentage of healthy lymph sites has dropped below 20% and an infected patient has succumbed to an opportunistic infection. However, the model is heading toward this equilibrium system before it reaches the third phase, so understanding this late phase is mathematically important; it is this third phase of the system that we study in this section.

As in Example 2.24, we view each site in the lattice as an independent Markov chain by modeling the orbit of an individual site using the probabilities generated by the three local rules. This point of view was taken by Hubbs (2006). Let $x \in X = \mathcal{A}^{\mathbb{Z}^2}$ be any point, and consider just the values that appear at the coordinate $x_{(0,0)}$ by following the local rules using $\tau = 4$. This produces the directed graph, G , in Fig. 27, where vertices represent the possible states in $\mathcal{A} = \{0, 1, 2, 3, 4, 5, 6\}$ and vertices i and j are connected by a directed edge if a cell in state i can transition to state j in one time step of the stochastic CA.

Let

$$A = \begin{pmatrix} 1 & 1 & 0 & 0 & 0 & 0 & 0 \\ 0 & 0 & 1 & 0 & 0 & 0 & 0 \\ 0 & 0 & 0 & 1 & 0 & 0 & 0 \\ 0 & 0 & 0 & 0 & 1 & 0 & 0 \\ 0 & 0 & 0 & 0 & 0 & 1 & 0 \\ 0 & 0 & 0 & 0 & 0 & 0 & 1 \\ 1 & 1 & 0 & 0 & 0 & 0 & 1 \end{pmatrix} \quad (23)$$

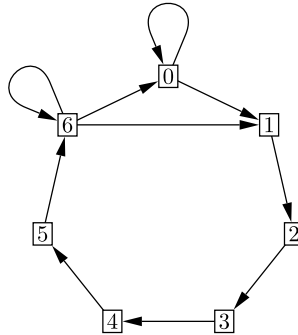


Fig. 27 Directed graph governing single state dynamics.

be the adjacency matrix of this graph. Then A defines a subshift (of finite type), $W_A \subseteq \mathcal{A}^{\mathbb{Z}^2}$, given by $W_A = \{w \in \mathcal{A}^{\mathbb{Z}^2} : a_{w_i w_{i+1}} = 1\}$.

We associate transition probabilities to the edges of G based on the associated update according to the local rules. Since f_j has the rules $1 \rightarrow 2, 2 \rightarrow 3, 3 \rightarrow 4, 4 \rightarrow 5,$ and $5 \rightarrow 6$, for all $j \in \{1, 2, 3\}$, these directed edges each have weight 1. The directed edges incident to 6 are weighted according to the probability of calling $f_1, f_2,$ or f_3 when the site is in state 6. Therefore, we weight the edge $6 \rightarrow 0$ with $p_1, 6 \rightarrow 1$ with $p_2,$ and $6 \rightarrow 6$ with p_3 ; these are the values arrived at biologically as explained in Sections 3 and 3.1. Finally, the weights of edges incident to 0 are determined by counting how many of the 7^8 total 3×3 patterns with a center 0 update to 0 and how many update to 1. The transitions are the same under each f_j , but depend on the parameter r . We compute the number of patterns which update to 0. For this to be the case, none of the 8 neighbors can have value 1, 2, 3, or 4, and so each neighbor must have value 0, 5, or 6. Further, there must be no more than r 5's and so we have $z(r) = \sum_{k=0}^{r-1} \binom{8}{k} 2^{8-k}$ of the 3×3 patterns with a center 0 which update to 0. Thus, $0 \rightarrow 0$ has weight $\frac{z(r)}{7^8}$ and $0 \rightarrow 1$ has weight $1 - \frac{z(r)}{7^8}$.

The stochastic transition matrices associated to each weighted, directed graph are the following:

$$P(r) = \begin{pmatrix} \frac{z(r)}{7^8} & 1 - \frac{z(r)}{7^8} & 0 & 0 & 0 & 0 & 0 \\ 0 & 0 & 1 & 0 & 0 & 0 & 0 \\ 0 & 0 & 0 & 1 & 0 & 0 & 0 \\ 0 & 0 & 0 & 0 & 1 & 0 & 0 \\ 0 & 0 & 0 & 0 & 0 & 1 & 0 \\ 0 & 0 & 0 & 0 & 0 & 0 & 1 \\ p_1 & p_2 & 0 & 0 & 0 & 0 & p_3 \end{pmatrix}. \tag{24}$$

Now we use $P(r)$ to obtain r shift-invariant Markov measures for the subshift W_A . Each $P(r), r \in \{2, 3, 4, 5, 6, 7, 8\}$, is a stochastic matrix, having a strictly positive probability vector $p(r)$ with $p(r)P(r) = p(r)$. Now as in Section 2.2, each probability vector, $p(r)$ can be used to obtain a shift-invariant Markov measure on $W_{P(r)}$. The values given in Eq. (24), obtained using values from primary sources and discussed in earlier sections of this paper, are: $p_3 = .01, p_2 = .99(10^{-5}),$ and $p_1 = .99 - p_2$.

Table 1 Vectors $p(r)$ with $p(r)P(r) = p(r)$

Value of r	Vector $p(r)$ with $p(r)P(r) = p(r)$
2	(0.142677, 142647, 142647, 142647, 142647, 142647, 144088)
4	(0.142753, 142634, 142634, 142634, 142634, 142634, 144075)
8	(0.142789, 142628, 142628, 142628, 142628, 142628, 144069)

For each fixed value of τ we note that for any $r = 2, \dots, 8$, the matrix in (24) is very close to (but never equal to) the matrix:

$$B = \begin{pmatrix} 0 & 1 & 0 & 0 & 0 & 0 & 0 \\ 0 & 0 & 1 & 0 & 0 & 0 & 0 \\ 0 & 0 & 0 & 1 & 0 & 0 & 0 \\ 0 & 0 & 0 & 0 & 1 & 0 & 0 \\ 0 & 0 & 0 & 0 & 0 & 1 & 0 \\ 0 & 0 & 0 & 0 & 0 & 0 & 1 \\ 1 & 0 & 0 & 0 & 0 & 0 & 0 \end{pmatrix}. \quad (25)$$

Note the difference between the matrices (24) and (25); it is easy to see that matrix B in (25) has left eigenvector $v = \{\frac{1}{7}, \dots, \frac{1}{7}\} \approx \{.142857, \dots, .142857\}$, and the left eigenvector corresponding to $P(r)$ in (24) for each value of r is very close to this with the first entry slightly smaller and the last slightly larger. In Table 1, we show the eigenvectors for several values of the parameter r .

The alphabet we have been using, $\mathcal{A} = \{0, 1, 2, 3, 4, 5, 6\}$, was determined by letting 0 represent a healthy site, letting 1 represent an initially infected A1 site, and then using values 2, 3, and 4 to represent the time lag from when an initially infected A1 site becomes an A2 infected site. This time lag is determined by τ , which we chose to be 4. However, τ can range from 2 to 6 (Zorzenon dos Santos and Coutinho, 2001), so we investigate the corresponding Markov shifts now. As τ varies, so does the size of the alphabet, and hence the directed graph determining the Markov shift. Let $\mathcal{A}_\tau = \{0, 1, \dots, \tau + 2\}$ be an alphabet for each $2 \leq \tau \leq 6$, where 0 and 1 are as before, $2, \dots, \tau$ capture the time lag, $\tau + 1$ represents an A2 infected site, and $\tau + 2$ represents a dead site. We then have the directed graphs G_τ , $\tau = 2, 3, 5, 6$, of Fig. 28.

Each directed graph has an adjacency matrix, P_τ , and each matrix, in turn, determines a subshift of finite type, W_τ , given by $W_\tau = \{w \in \mathcal{A}_\tau^{\mathbb{Z}} : (P_\tau)_{w_i w_{i+1}} = 1\}$. Transition probabilities are assigned to the directed edges as follows. In each case, the rules $1 \rightarrow 2, 2 \rightarrow 3, \dots, (\tau + 1) \rightarrow (\tau + 2)$ are fixed, and thus these all have transition probability 1. The rules $(\tau + 2) \rightarrow 0, (\tau + 2) \rightarrow 1$, and $(\tau + 2) \rightarrow (\tau + 2)$ occur according to the probabilities p_1, p_2 , and p_3 , respectively, independent of the value of τ , so we assign these weights. To determine the weight of the $0 \rightarrow 0$ edge, we consider a 3×3 block over \mathcal{A}_τ having a center 0, and count the number of these blocks which update to 0 according to the local rules, f_1, f_2 , and f_3 . Again, the transitions are the same under each f_j , but depend on the parameter r . For a 0 to remain a 0, none of the 8 neighbors may have an A1 infected value of $1, 2, \dots, \tau$, and so each neighbor must have value 0, $\tau + 1$, or $\tau + 2$. Since there must be no more than r of the A2 infected value, $\tau + 1$, we have $z(r) = \sum_{k=0}^{r-1} \binom{8}{k} 2^{8-k}$ of the 3×3 patterns with a center 0 which update to 0, as before. However, there are $(\tau + 3)^8$

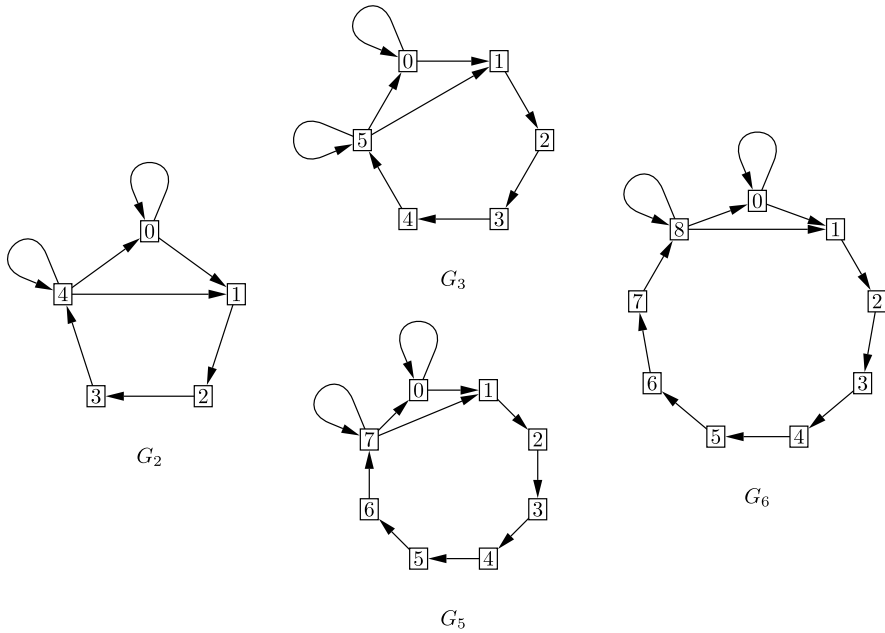


Fig. 28 Directed graphs governing single state dynamics for $2 \leq \tau \leq 6$.

total 3×3 patterns over \mathcal{A}_τ , and so the probabilities depend on both r and τ . We have $0 \rightarrow 0$ with weight $\frac{z(r)}{(\tau+3)^8}$ and $0 \rightarrow 1$ with weight $1 - \frac{z(r)}{(\tau+3)^8}$.

Then to each pair τ, r , we associate a stochastic matrix, $P(\tau, r)$, coming from the probabilities given above. As before, we compute the positive probability vector, $p(\tau, r)$, satisfying $p(\tau, r)P(\tau, r) = p(\tau, r)$. Each $p(\tau, r)$ determines a shift-invariant Markov measure on W_τ . In each case, we obtain a vector

$$p(\tau, r) \approx \left(\frac{1}{\tau+3}, \dots, \frac{1}{\tau+3} \right).$$

The largest percentage of healthy cells occurs as the first entry in the vector:

$$p(2, 8) \approx (0.202315, .198919, .198919, .198919, .200928),$$

and we note that this is still below the threshold for surviving the viral infection. This supports the clinical findings that without drug therapy an individual’s chances for surviving the HIV infection are essentially nil.

6. The effect of drug therapy on the model

We describe briefly the mechanisms of current drug treatment as outlined by Nowak and May (2000), and show how our CA model can be modified to reflect the effects of some

of the recent treatment therapies. The earliest drug, zidovudine (or AZT), is a reverse transcriptase inhibitor which prevents the virus from copying its RNA into DNA for insertion into the host cell. After application of AZT, the $CD4^+$ T cell count increases sharply within 2 weeks, but the effects are short-lived due to viral mutations. There have been improvements in reverse transcriptase inhibitors and they are still used today. Most current drug therapy has moved beyond a single drug to combination drug therapy, which uses several types of reverse transcriptase inhibitors along with a protease inhibitor. In brief, protease inhibitors prevent virus particles leaving an infected cell from being able to infect new cells and are designed to act on virus particles that escape the first drug. There is a detailed discussion of how drug therapy affects an ordinary differential equations model in Nowak and May (2000). Here, we give a simple approximation to how it can be incorporated into our stochastic CA model. Due to the simplistic assumptions, we do not go back to the primary references; our working assumption is that drugs are designed to prevent infected cells from infecting nearby cells through one of the two mechanisms mentioned above: by either reverse transcriptase inhibitors or protease inhibitors and both drugs are used.

We claim that the rapid mutation of the virus, made more pronounced by the reaction of the virus to drug therapy (Nowak and May, 2000), introduces randomness into the model earlier and pushes us into Phase 3 dynamics much faster. The point of view we take with our math model of the viral spread then is the following; we modify the model not so that the latency period is longer, but instead *we head straight to Phase 3 dynamics and see what is needed to cause the limiting behavior of the dynamical system to asymptotically approach a larger percentage of healthy cells*. In this way, we control the limiting percentages of the $CD4^+$ T cell population and ultimately the long term health of the patient by heading toward a desirable final equilibrium state of the total system, instead of studying each individual cell or site. We explain this by giving an example.

Suppose that at each time step, with some positive probability, an infected cell returns to the healthy state. This happens in one of two ways due to the drug therapy: either the infected cell releases malformed viral particles that can do no further harm and is replenished by a healthy cell, or it dies without infecting any neighboring cells and is simply replenished by a healthy one. However, by definition of infected A_2 , (which is an infected cell that has been able to infect its neighbors for some time), we will assume that if a site is in state $m - 1$ then it will always die at the next time step. Then the incidence matrix is as follows and we compare it to the matrices A and B in (23): Let

$$C = \begin{pmatrix} 1 & 1 & 0 & 0 & 0 & 0 & 0 \\ 1 & 0 & 1 & 0 & 0 & 0 & 0 \\ 1 & 0 & 0 & 1 & 0 & 0 & 0 \\ 1 & 0 & 0 & 0 & 1 & 0 & 0 \\ 1 & 0 & 0 & 0 & 0 & 1 & 0 \\ 0 & 0 & 0 & 0 & 0 & 0 & 1 \\ 1 & 1 & 0 & 0 & 0 & 0 & 1 \end{pmatrix}. \quad (26)$$

Therefore, C defines a subshift of finite type, $W_C \subseteq \mathcal{A}^{\mathbb{Z}^2}$. We now use some hypothetical assumptions to proceed to the associated stochastic matrix for the incidence matrix C (using $r = 4$). We first suppose that the drug is only 25% effective in preventing an uninfected cell contiguous to an infected cell to become infected by the virus. Therefore, in

1 week's time, this has occurred for three generations already, so only $.75^3 \sim 42.2\%$ of the cells that would have been infected are indeed infected. We next suppose that after each week passes, the effectiveness of the drugs are such that half of the infected cells are infected with virus that is not properly functioning so the cell dies and is replaced by a healthy one. The other half just continue infecting neighbors 75% of the time since our assumption is that the two types of drugs are administered simultaneously. Then the associated stochastic matrix for C is as follows:

$$Q = \begin{pmatrix} .578 + .422\frac{z(r)}{7^8} & .422(1 - \frac{z(r)}{7^8}) & 0 & 0 & 0 & 0 & 0 & 0 \\ 0.5 & 0 & 0.5 & 0 & 0 & 0 & 0 & 0 \\ 0.5 & 0 & 0 & 0.5 & 0 & 0 & 0 & 0 \\ 0.5 & 0 & 0 & 0 & 0.5 & 0 & 0 & 0 \\ 0.5 & 0 & 0 & 0 & 0 & 0.5 & 0 & 0 \\ 0 & 0 & 0 & 0 & 0 & 0 & 0 & 1 \\ p_1 & p_2 & 0 & 0 & 0 & 0 & 0 & p_3 \end{pmatrix} \tag{27}$$

or, making the calculations using $r = 4$, we have (q, Q) Markov shifts with

$$Q = \begin{pmatrix} .5784 & .4216 & 0 & 0 & 0 & 0 & 0 & 0 \\ 0.5 & 0 & 0.5 & 0 & 0 & 0 & 0 & 0 \\ 0.5 & 0 & 0 & 0.5 & 0 & 0 & 0 & 0 \\ 0.5 & 0 & 0 & 0 & 0.5 & 0 & 0 & 0 \\ 0.5 & 0 & 0 & 0 & 0 & 0.5 & 0 & 0 \\ 0 & 0 & 0 & 0 & 0 & 0 & 0 & 1 \\ .98999 & 9.9 \times 10^{-6} & 0 & 0 & 0 & 0 & 0 & .01 \end{pmatrix} \tag{28}$$

and left eigenvector

$$q \approx (0.54248, 0.22869, 0.11435, 0.057172, 0.028586, 0.014293, 0.014293, 0.014437).$$

Since the leading entry is around 54% and gives the long term steady state percentage of healthy cells, this shows a much better prognosis for the patient. There are many factors that are not taken into account when doing this drug therapy model, but the analysis indicates some ways in which the model can best support the advances in drug therapy for infected individuals and suggests some directions for future research.

Acknowledgements

The first author was supported by the Santa Fe Institute when most of this work was carried out.

References

Allouche, J., Courbage, M., Skordev, G., 2001. Notes on cellular automata. *Cubo Mat. Educ.* 3(2), 213–244.

- Bernaschi, M., Castiglione, F., 2002. Selection of escape mutants from the immune recognition during HIV infection. *Immunol. Cell Biol.* 80, 307–313.
- Blanchard, F., Tisseur, P., 2000. Some properties of cellular automata with equicontinuity points. *Ann. Inst. Henri Poincaré Probab. Stat.* 36(5), 569–582.
- Fauci, A., Pantaleo, G., Stanley, S., Weissman, D., 1996. Immunopathogenic mechanisms of HIV infection. *Ann. Int. Med.* 124(7), 654–663.
- Feinberg, M.B., 2002. The interface between the pathogenesis and treatment of HIV infection. In: *The Human Immunodeficiency Virus: Biology, Immunology, and Therapy*, pp. 384–440. Princeton University Press, Princeton.
- Gamber, E., 2006. Equicontinuity properties of D-dimensional cellular automata. *Topol. Proc.* 30(1), 197–222. Spring Topology and Dynamical Systems Conference.
- Gamber Burkhead, E., 2008. A topological classification of D-dimensional cellular automata. *Dyn. Syst. Int. J.* to appear
- Haase, A.T., 1999. Population biology of HIV-1 infection: Viral and $CD4^+$ T cell demographics and dynamics in lymphatic tissues. *Annu. Rev. Immunol.* 17, 625–656.
- Hawkins, J., Molinek, D., 2007. One-dimensional stochastic cellular automata. *Topol. Proc.* 31(2), 515–532.
- Hedlund, G.A., 1969. Endomorphisms and automorphisms of the shift dynamical system. *Math. Syst. Theory* 3, 320–375.
- Hubbs, J., 2006. A probabilistic cellular automaton model of the spread of the HIV virus. Master's project. University of North Carolina at Chapel Hill.
- Ilachinski, A., 2001. Cellular automata. A discrete universe. World Scientific, River Edge.
- Kari, J., 2005. Theory of cellular automata: A survey. *Theor. Comput. Sci.* 334, 3–33.
- Kitchens, B.P., 1998. Symbolic dynamics: one-sided, two-sided and countable state Markov shifts. Universitext, Springer, Berlin.
- Kůrka, P., 2001. Topological dynamics of cellular automata. In: *Codes, Systems, and Graphical Models (Minneapolis, MN, 1999)*. IMA Vol. Math. Appl., vol. 123, pp. 447–485. Springer, Berlin
- Lind, D., Marcus, B., 1995. An introduction to symbolic dynamics and coding. Cambridge University Press, Cambridge.
- Nowak, M.A., May, R.M., 2000. Virus dynamics. Mathematical principles of immunology and virology. Oxford University Press, Oxford.
- Pantaleo, G., Fauci, A.S., 1996. Immunopathogenesis of HIV infection. *Ann. Rev. Microbiol.* 50, 825–854.
- Pantaleo, G., Graziosi, C., Fauci, A., 1993. The immunopathogenesis of human immunodeficiency virus infection. *New Engl. J. Med.* 328(5), 327–335.
- Schnittman, S.M., et al., 1989. The reservoir for HIV-1 in human peripheral blood is a T cell that maintains expression of CD4. *Science* 245(4915), 305–308.
- Sinai, Y.G., 1994. Topics in ergodic theory, Volume 44 of Princeton Mathematical Series. Princeton University Press, Princeton.
- Strain, M.C., Levine, H., 2002. Comment on “Dynamics of HIV infection: A cellular automata approach”. *Phys. Rev. Lett.* 89(21), 219805–1.
- Walters, P., 1982. An introduction to ergodic theory. Springer, Berlin.
- Wolfram, S., 1984. Universality and complexity in cellular automata. *Physica D* 10(1–2), 1–35. Cellular automata (Los Alamos, NM, 1983).
- Wolfram, S., 2002. A new kind of science. Wolfram Media, Champaign.
- Zhang, Z.-Q., et al., 1998. Kinetics of $CD4^+$ T cell repopulation by lymphoid tissues after treatment of HIV-1 infection. *Proc. Natl. Acad. Sci.* 95, 1154–1159.
- Zorzenon dos Santos, R.M., Coutinho, S., 2001. Dynamics of HIV infection: A cellular automata approach. *Phys. Rev. Lett.* 87(16), 168102-1–168102-4.